

Localized stem structures in soliton reconnection of the asymmetric Nizhnik-Novikov-Veselov system

Feng Yuan^{a,**}, Jingsong He^{c,*}, Yi Cheng^c

^aCollege of Science, Nanjing University of Posts and Telecommunications, Nanjing, 210023, P. R. China

^bInstitute for Advanced Study, Shenzhen University, Shenzhen, 518060, P. R. China

^cSchool of Mathematical Sciences, USTC, Hefei, Anhui 230026, P. R. China

Abstract

The reconnection processes of 3-solitons with 2-resonance can produce distinct local structures that initially connect two pairs of V-shaped branches, then disappear, and later re-emerge as new forms. We call such local structures as stem structures. In this paper, we investigate the variable-length stem structures during the soliton reconnection of the asymmetric Nizhnik-Novikov-Veselov system. We consider two scenarios: weak 2-resonances (i.e., $a_{12} = a_{13} = 0$, $0 < a_{23} < +\infty$) and strong 2-resonances (i.e., $a_{12} = a_{13} = +\infty$, $0 < a_{23} < +\infty$). We determine the asymptotic forms of the four arms and their corresponding stem structures using two-variable asymptotic analysis method which is involved simultaneously with one space variable y (or x) and one temporal variable t . Different from known studies, our findings reveal that the asymptotic forms of the arms S_2 and S_3 differ by a phase shift as $t \rightarrow \pm\infty$. Building on these asymptotic forms, we perform a detailed analysis of the trajectories, amplitudes, and velocities of the soliton arms and stem structures. Subsequently, we discuss the localization of the stem structures, focusing on their endpoints, lengths, and extreme points in both weak and strong 2-resonance scenarios.

Keywords: Two-variable asymptotic analysis method; Localized stem structure; Resonant collision; Soliton reconnection.

1. Introduction

Soliton theory is an important research area in the nonlinear science, focusing on a particular type of nonlinear wave known as a solitary wave. The solitary wave was first observed by J. S. Russell [1] in a canal and later explained by the KdV equation formulated by Korteweg and de Vries [2]. After colliding, two solitary waves can return to their original shapes and conserve their momentums and energies, which satisfies the properties of elastic collisions [3–7]. This “particle-like” behavior of solitary waves is a crucial characteristic corresponding to their naming term “soliton”.

In physics, solitons emerge as distinctive manifestations of nonlinear phenomena. Endowed with unique attributes including conservation of energy, momentum preservation, and stability, solitons find extensive application across diverse fields of physics [3]. Mathematically, solitons are defined as stable and energy-conserving non-dispersive solutions within specific nonlinear partial differential equations. Soliton equations serve as mathematical models for describing the essences and characteristics of solitons. In a seminal contribution in 1965, Zabusky and Kruskal introduced the concept of solitons for the KdV equation through numerical method [7]. Two years later, a method of solving the initial value problem of

*Corresponding author. E-mails: hejingsong@szu.edu.cn

**Corresponding author. E-mails: fengyuan@njupt.edu.cn

the KdV equation was proposed in Ref. [8], which also (or further) produces a closed form of n soliton solutions. This method is now widely known as inverse scattering method. Subsequently, in 1974, the exact and analytical n -soliton solutions for the KdV equation were successfully derived utilizing inverse scattering method [4]. Since then, numerous soliton equations have been discovered [3, 5, 7], and other analytical methods have been developed for solving these equations, including the Darboux transformation [9–11], and the Hirota bilinear method [12, 13].

The study of soliton interactions is a key research focus in soliton theory. While elastic collisions are a fundamental feature of solitons, solitons may also undergo inelastic collisions [14–16] under special conditions. A distinctive class of “resonant” interactions arises when the wave numbers and frequencies of solitons meet specific constraints, first identified in the context of the Kadomtsev-Petviashvili (KP) equation [17–21]. Resonance is generated through two main mechanisms: (i) resonance occurs when the intersection angle of solitons meets certain conditions [22]; (ii) resonance arises when the phase shift becomes indefinite [23–25]. In this study, we examine soliton interactions from the perspective of phase shift: elastic collisions exhibit a finite phase shift, while resonant collisions are characterized by an infinite phase shift. Furthermore, when the phase shift in an elastic collision is finite but approaches infinity, it is termed as a quasi-resonant collision.

Commonly speaking, two-dimensional line solitons extend infinitely in space. However, quasi-resonant and resonant collisions can give rise to localized stem structures. The concept of the stem structure was first introduced in the context of Mach reflection [17, 26]. In this phenomenon, the apex of the incident and reflected wave separates from the wall and is connected to it by a third solitary wave that perpendicularly intersects the wall, now widely known as the stem wave. In the quasi-resonant state, the vertices of the X-shaped solitons are significantly separated due to the phase delay, forming two V-shaped solitons connected by a new localized structure, as another instance of the stem structure [27]. Additionally, the 3-soliton can produce a localized structure when it resonates twice. In this scenario, the soliton appears as four surrounding infinity arms connected by an intermediate soliton (stem structure). Over time, the middle soliton gradually shrinks, resulting in the merge of the endpoints of the other four arms. They later separate again and are reconnected by a new middle soliton with a different orientation. The entire process is known as the soliton reconnection [24, 28, 29]. The common features of both quasi-resonant and soliton reconnection are the localization and finite length of the stem structures.

In this study, we define the stem structure (or wave) as a localized wave connecting the vertices of two pairs of V-shaped line solitons. Spatial localization is the fundamental characteristic of the stem structure. Investigating the stem structure in solitons can provide deeper insights into the nature of solitons and enhances our understanding of various nonlinear phenomena. The stem structure has been studied to some extent in solitons by a graphic way without analytic formulas of the stem structures. For example:

- In the case of 2-solitons for the KP equation and the Boussinesq equation, the central region of the X-shaped soliton forms a constant-length stem when the phase shift is finitely large [22, 23, 30].
- For 3-solitons in the KP and Davey-Stewartson (DS) equations, soliton reconnection generates two finite structures: during this process, one finite structure gradually disappears while another emerges [24, 29].

Although various equations describe the two types of soliton collisions resulting from interactions [23, 31–34], there has been limited analysis of the stem structure of solitons, aside from some intuitive and interesting graphical demonstrations. In this work, we choose the asymmetric Nizhnik-Novikov-Veselov (ANNV) system to analytically study the localized stem structures in 3-solitons, primarily due to its significant applications in numerous fields of physics, especially in shallow waves driven by weakly nonlinear restoring forces in incompressible fluids [35, 36]. This system was originally introduced by

Boiti utilizing the weak Lax pair [37], and it has the following form:

$$\begin{cases} u_t + v_{xxx} = 3(uv)_x, \\ u_x = v_y. \end{cases} \quad (1.1)$$

Here, $u(x, y, t)$ and $v(x, y, t)$ denote the dimensionless velocity components. The spectral transformation for this system has been investigated in Ref. [3, 37]. It has been shown that when $x = y$, Eq. (1.1) simplifies to the KdV equation [37]. Additionally, this system can be derived through the inner parameter-dependent symmetry constraint of the KP equation [35]. Clarkson and Mansfield have investigated several crucial aspects of the ANNV system, including the Painlevé property and similarity solutions [38]. Furthermore, a plethora of solution types has been delineated in the past researches. Dromion and kink solutions have been meticulously crafted and documented in the seminal works of [36, 39]. Notably, the quasi-periodic solutions have been rigorously formulated in the scholarly discourse outlined in Ref. [40]. Similarly, soliton solutions have been meticulously derived and discussed in the scholarly investigation chronicled in Ref. [41]. Moreover, lump solution has been exhaustively examined and elucidated in the comprehensive research efforts documented in Refs. [42]. Finally, the elucidation of rational and semi-rational solutions has been systematically undertaken in the insightful analysis presented in Refs. [43, 44].

Recently, the quasi-resonant 2-solitons with constant-length stem structures have been constructed and studied in Ref. [45]. However, the 2-resonant 3-soliton solution of Eq. 1.1, which produces a variable-length stem structure during soliton reconnection, has not been explored. The essential challenges in this study on stem structures are as follows:

- How to consider the asymptotic analysis involved simultaneously with one space variable y (or x) and one temporal variable t in two dimensional solitons? There are many known results on the asymptotic analysis just on only one spatial variable (x or y) [19, 46] or on time variable t [47, 48], which cannot provide the accurate form of soliton arms. This two-variable asymptotic analysis method is crucial to determine ends of stem structures and find the accurate form of soliton arms before and after the interactions of multi-soliton.
- Based on the accurate form of soliton arms, how to find the analytical forms for the ends, length, trajectory of the stem structures?

The primary objective is to overcome the above challenges and to study the variable-length stem structure in 2-resonant 3-soliton solutions. Unlike the resonant solution derived in Ref. [24] by transforming the polar coordinates of x and y and subsequently controlling the angle between them, our study induces soliton reconnection by satisfying the 2-resonance condition for two of the three a_{ij} . The solutions obtained in our paper resemble the partially resonant solutions described in Ref. [24] (subsection 7.2). We will demonstrate that the 2-resonance condition [19] implies that resonance will occur at two different points on the (x, y) -plane. Furthermore, soliton reconnections manifest in two cases: weak and strong resonances, distinguished by whether $a_{ij} = 0$ or $a_{ij} = \infty$. It is worth noting that due to the extremely complex interaction mechanism of multi-solitons near $t = 0$, which has not yet been fully characterized, the asymptotic analysis of 2-resonant 3-solitons and the research on stem structures conducted in this paper are only applicable to the cases of $t \ll 0$ and $t \gg 0$. The organization of the paper is as follows: In Sec. 2, we recall the expressions and N-solution for the ANNV equation (1.1) based on the Hirota Bilinear method. In Secs. 3 and 4, we delve into the asymptotic forms and the stem structure in 3-soliton solutions generated by weak 2-resonance and strong 2-resonance, respectively, exploring soliton reconnection and studying the properties of the variable-length stem structures produced during reconnection. Finally, in Sec. 5, we provide conclusions and discussions for this paper.

Table 1: Physical quantities of the soliton

Soliton	Trajectory	Velocity	Amplitude	Components
S_j	l_j	$(k_j^2, -\frac{k_j}{p_j})$	$-\frac{k_j p_j}{2k_j^2}$	u_j v_j
S_j	\widehat{l}_j	$(k_j^2, -\frac{k_j}{p_j})$	$-\frac{k_j p_j}{2k_j^2}$	\widehat{u}_j \widehat{v}_j

The j -th soliton S_j ($j = 1, 2, 3$) is composed by two components u_j and v_j , and their essential properties are summarized in Table 1. The trajectories of the three kinds of solitons S_j are given by (3.9).

2. Recall the N-soliton solutions of the ANNV system

The N-soliton solutions of (1.1) generated by the Hirota Bilinear method have been given by [49]

$$u = -2(\ln f)_{xx}, \quad v = -2(\ln f)_{xy}, \quad (2.1)$$

$$f^{[N]} = \sum_{\mu=0,1} \exp \left(\sum_{i < j}^N \mu_i \mu_j A_{ij} + \sum_{i=1}^N \mu_i \xi_i \right), \quad (2.2)$$

where,

$$\xi_j = k_j x + p_j y - k_j^3 t + \xi_j^0, \quad \exp(A_{ij}) = \frac{(k_i - k_j)(p_i - p_j)}{(k_i + k_j)(p_i + p_j)} \triangleq a_{ij} \geq 0. \quad (2.3)$$

By substituting $N = 3$ into Eq. (2.2), the order-3 soliton solution can be derived using (2.1) and the subsequent equation:

$$\begin{aligned} f^{[3]} = & 1 + \exp \xi_1 + \exp \xi_2 + \exp \xi_3 + a_{12} \exp(\xi_1 + \xi_2) + a_{13} \exp(\xi_1 + \xi_3) \\ & + a_{23} \exp(\xi_2 + \xi_3) + a_{12} a_{13} a_{23} \exp(\xi_1 + \xi_2 + \xi_3). \end{aligned} \quad (2.4)$$

The phase shift of the 3-soliton solution is denoted as $\Delta_{ij} = \ln a_{ij}$ for $(i, j = 1, 2, 3 \text{ and } i < j)$. Different conditions on the phase shift give rise to distinct types of collisions between the three solitons: elastic collisions for $\Delta_{ij} < \infty$, and resonant collisions for $\Delta_{ij} = \infty$. In this paper, we narrow our focus to the variable-length stem structure in 3-solitons by 2-resonance, occurring when $a_{12} = a_{13} = 0$ or $a_{12}, a_{13} = \infty$. Here, the 2-resonance condition denotes that resonance can occur twice at different points on the (x, y) -plane. The weak resonance corresponds to $a_{ij} = 0$, and the strong resonance corresponds to $a_{ij} = +\infty$.

Remark 2.1. *The distinction between strong and weak resonances lies in their outcomes: strong resonance between S_i ($f_i = 1 + \exp \xi_i$) and S_j ($f_j = 1 + \exp \xi_j$) produce a soliton S_{i+j} ($f_{i+j} = 1 + \exp(\xi_i + \xi_j)$), whereas weak resonance yield S_{i-j} ($f_{i-j} = 1 + \exp(\xi_i - \xi_j)$).*

Remark 2.2. *The interaction mechanism of multi-solitons in the neighborhood of $t = 0$ is extremely complex and has not yet been fully described. Based on this, the research on the asymptotic forms and stem structures of 2-resonance 3-solitons carried out in this paper only holds under the conditions of $t \ll 0$ and $t \gg 0$.*

3. The stem structure in 3-soliton generated by weak 2-resonance in soliton reconnection

In this section, we focus on the 3-soliton generated by weak 2-resonance in the case of $a_{12} = a_{13} = 0$ and $0 < a_{23} < +\infty$, during the soliton reconnection. The corresponding transformation of Eq. (2.4) is captured by the expression:

$$f_{weak} = 1 + \exp \xi_1 + \exp \xi_2 + \exp \xi_3 + a_{23} \exp(\xi_2 + \xi_3). \quad (3.1)$$

To delve into the 3-soliton solution with weak 2-resonance, as defined by Eqs. (3.1) and (2.1), we explore its asymptotic behavior by two-variable asymptotic analysis, which is involved with y and t . In order to satisfy the condition $a_{12} = a_{13} = 0$, $0 < a_{23} < +\infty$, without loss of generality, we will discuss it in two cases: (1) $0 < k_1 = k_3 < k_2$, $p_1 = p_2 > p_3 > 0$ and (2) $k_1 = k_2 > k_3 > 0$, $0 < p_1 = p_3 < p_2$.

3.1. The asymptotic analysis with $0 < k_1 = k_3 < k_2$, $p_1 = p_2 > p_3 > 0$

Previous researches on asymptotic analysis considering the asymptotic behaviors of the spatial variables and treats t as a constant [19, 46–48], producing only static asymptotic forms. Note that the parameters c and c_j introduced in the asymptotic analysis in this paper do not refer to specific values but rather to general constants.

First, we use t as a constant as the asymptotic analysis in Refs. [19, 46–48], in order to show clearly that the description of soliton arms is not accurate due to the different appearance of phase shift terms, by the known way. We consider the region $\zeta_j = x + \frac{p_j}{k_j}y = \text{constant}$:

(1) When $y \rightarrow -\infty$, we have $\eta_1 \approx c$, $\eta_2 \rightarrow +\infty$, $\eta_3 \rightarrow +\infty$, $\eta_2 \gg \eta_3$, and then $f \approx \exp(\eta_2) + a_{23} \exp(\eta_2 + \eta_3)$.

(2) When $y \rightarrow +\infty$, we have $\eta_1 \approx c$, $\eta_2 \rightarrow -\infty$, $\eta_3 \rightarrow -\infty$, $\eta_2 + \eta_3 \rightarrow -\infty$, and then $f \approx 1 + \exp(\eta_1)$.

(3) When $y \rightarrow -\infty$ we have $\eta_2 \approx c$, $\eta_1 \rightarrow -\infty$, $\eta_3 \rightarrow -\infty$, $\eta_2 + \eta_3 \rightarrow -\infty$, and then $f \approx 1 + \exp(\eta_2)$.

(4) When $y \rightarrow +\infty$, we have $\eta_2 \approx c$, $\eta_1 \rightarrow +\infty$, $\eta_3 \rightarrow +\infty$, $\eta_2 + \eta_3 \rightarrow +\infty$, $\eta_1 \gg \eta_3$, and then $f \approx \exp(\eta_1) + a_{23} \exp(\eta_2 + \eta_3)$.

(5) When $y \rightarrow -\infty$, we have $\eta_3 \approx c$, $\eta_1 \rightarrow -\infty$, $\eta_2 \rightarrow +\infty$, $\eta_2 + \eta_3 \rightarrow +\infty$, and then $f \approx \exp(\eta_2) + a_{23} \exp(\eta_2 + \eta_3)$.

(6) When $y \rightarrow +\infty$, we have $\eta_3 \approx c$, $\eta_1 \rightarrow +\infty$, $\eta_2 \rightarrow -\infty$, $\eta_2 + \eta_3 \rightarrow -\infty$, and then $f \approx \exp(\eta_1)$.

After sorting above analysis out, we have the following asymptotic forms,

$$\begin{aligned} f_2 &\sim 1 + e^{\eta_2}, f_3 \sim 1 + a_{23}e^{\eta_3}, (y \rightarrow -\infty), \\ f_1 &\sim 1 + e^{\eta_1}, f_{1-2-3} \sim 1 + a_{23}e^{\eta_2+\eta_3-\eta_1}, (y \rightarrow +\infty). \end{aligned} \quad (3.2)$$

In fact, the asymptotic forms obtained here are not accurate and cannot reflect the temporal attributes of the asymptotic forms at $t \rightarrow \pm\infty$. The accurate asymptotic forms will be given in (3.3) as $t \rightarrow -\infty$ and (3.4) as $t \rightarrow +\infty$, which includes different appearance of phase shift term a_{23} . This difference of u between t goes to $\pm\infty$ is very crucial to understand the asymptotic behavior of u . This verifies that asymptotic from in (3.2), does not provide a accurate form of soliton arms, and shows it is necessary to use two-variable asymptotic method in this paper. Specifically, in a 2-resonant 3-soliton solution, some arms experience a phase shift as $t \rightarrow -\infty$ or $t \rightarrow +\infty$ due to the influence of a_{23} . In this paper, the asymptotic analysis we undertake necessitates a concurrent examination of both a spatial variable y and a temporal variable t , a methodology referred to in the paper as two-variable asymptotic analysis method. To be convenient, we consider the region $\eta_j = x + \frac{p_j}{k_j}y - k_j^2t = \text{constant}$ instead of $\zeta_j = x + \frac{p_j}{k_j}y = \text{constant}$. The former allows η_j to be treated as a constant for any variable, while the latter requires t to be constant to treat ζ_j as a constant.

I. On the region $\eta_1 = x + \frac{p_1}{k_1}y - k_1^2t$, we have

$$\xi_1 = k_1\eta_1 + c_1, \xi_2 = k_2\eta_1 + \frac{k_1p_2 - k_2p_1}{k_1}y + k_2(k_1^2 - k_2^2)t + c_2, \xi_3 = k_3\eta_1 + \frac{k_1p_3 - k_3p_1}{k_1}y + c_3,$$

$$\xi_2 + \xi_3 = (k_2 + k_3)\eta_1 + \frac{(p_2 + p_3)k_1 - p_1(k_2 + k_3)}{k_1}y + ((k_2 + k_3)k_1^2 - (k_2^3 + k_3^3))t + c_4.$$

(a) In the case of $t \rightarrow +\infty$: We have $\xi_1 \approx c$, $\xi_2 \rightarrow -\infty$, $\xi_3 \approx c$, $\xi_2 + \xi_3 \rightarrow -\infty$, and then Eq. (3.1) becomes $f \sim 1 + e^{\xi_1} + e^{\xi_3}$. Further we can get:

$$f \sim 1 + e^{\xi_1}, y \rightarrow +\infty; f \sim 1 + e^{\xi_3}, y \rightarrow -\infty; f \sim e^{\xi_1} + e^{\xi_3}, x \rightarrow +\infty.$$

(b) In the case of $t \rightarrow -\infty$, $y \rightarrow -\infty$: We have $\xi_1 \approx c$, $\xi_2 \rightarrow +\infty$, $\xi_3 \rightarrow +\infty$, $\xi_2 + \xi_3 \rightarrow +\infty$. Because of $\xi_2 - \xi_3 = (k_2 - k_3)\eta_1 + \frac{k_1 p_2 - k_2 p_1 - k_1 p_3 + k_3 p_1}{k_1}y + k_2(k_1^2 - k_2^2)t \rightarrow +\infty$ for $t \rightarrow -\infty$, $y \rightarrow -\infty$, we have $e^{\xi_2} + a_{23}e^{\xi_2 + \xi_3} \gg e^{\xi_3}$. And then we can get:

$$f \sim e^{\xi_2} + a_{23}e^{\xi_2 + \xi_3}, t \rightarrow -\infty, y \rightarrow -\infty.$$

(c) In the case of $t \rightarrow -\infty$, $y \rightarrow +\infty$: By the limit $y \rightarrow +\infty$, we have $\xi_1 \approx c$, $\xi_2 \rightarrow -\infty$, $\xi_3 \rightarrow -\infty$, $\xi_2 + \xi_3 \rightarrow -\infty$. Since a_{23} is not applied to soliton S_1 , we get $f \sim 1 + e^{\xi_1}$, $y \rightarrow +\infty$ for even t .

II. On the region $\eta_2 = x + \frac{p_2}{k_2}y - k_2^2 t$, we have

$$\xi_1 = k_1\eta_2 + \frac{k_2 p_1 - k_1 p_2}{k_2}y + k_1(k_2^2 - k_1^2)t + c_1, \xi_2 = k_2\eta_2 + c_2, \xi_3 = k_3\eta_2 + \frac{k_2 p_3 - k_3 p_2}{k_2}y + k_3(k_2^2 - k_3^2)t + c_3,$$

$$\xi_2 + \xi_3 = (k_2 + k_3)\eta_2 + \frac{k_2 p_3 - k_3 p_2}{k_2}y + k_3(k_2^2 - k_3^2)t + c_4.$$

(a) In the case of $t \rightarrow +\infty$: We have $\xi_2 \approx c$, $\xi_1 \rightarrow +\infty$, $\xi_3 \rightarrow +\infty$, $\xi_2 + \xi_3 \rightarrow +\infty$, and then Eq. (3.1) becomes $f \sim e^{\xi_1} + e^{\xi_3} + a_{23}e^{\xi_2 + \xi_3}$. Further we can get:

$$f \sim e^{\xi_3} + a_{23}e^{\xi_2 + \xi_3}, y \rightarrow -\infty; f \sim e^{\xi_1} + a_{23}e^{\xi_2 + \xi_3}, y \rightarrow +\infty; f \sim e^{\xi_1} + e^{\xi_3}, x \rightarrow -\infty.$$

(b) In the case of $t \rightarrow -\infty$, $y \rightarrow -\infty$: We have $\xi_2 \approx c$, $\xi_1 \rightarrow -\infty$, $\xi_3 \rightarrow -\infty$, $\xi_2 + \xi_3 \rightarrow -\infty$, and then Eq. (3.1) becomes

$$f \sim 1 + e^{\xi_2}, t \rightarrow -\infty, y \rightarrow -\infty.$$

(c) In the case of $t \rightarrow -\infty$, $y \rightarrow +\infty$: By the limit $y \rightarrow +\infty$, we have $\xi_2 \approx c$, $\xi_1 \rightarrow +\infty$, $\xi_3 \rightarrow +\infty$, $\xi_2 + \xi_3 \rightarrow +\infty$ and $f \sim e^{\xi_1} + e^{\xi_3} + a_{23}e^{\xi_2 + \xi_3}$. Because of $\xi_3 - \xi_1 = (k_3 - k_1)\eta_2 + (p_3 - p_1)y \rightarrow -\infty$, we have $e^{\xi_1} + a_{23}e^{\xi_2 + \xi_3} \gg e^{\xi_3}$. So $f \sim e^{\xi_1} + a_{23}e^{\xi_2 + \xi_3}$, $y \rightarrow +\infty$ for even t .

III. On the region $\eta_3 = x + \frac{p_3}{k_3}y - k_3^2 t$, we have

$$\xi_1 = k_1\eta_3 + \frac{k_3 p_1 - k_1 p_3}{k_3}y + c_1, \xi_2 = k_2\eta_3 + \frac{k_3 p_2 - k_2 p_3}{k_3}y + k_2(k_3^2 - k_2^2)t + c_2, \xi_3 = k_3\eta_3 + c_3,$$

$$\xi_2 + \xi_3 = (k_2 + k_3)\eta_1 + \frac{k_3 p_2 - k_2 p_3}{k_3}y + k_2(k_3^2 - k_2^2)t + c_4.$$

(a) In the case of $t \rightarrow +\infty$: We have $\xi_3 \approx c$, $\xi_1 \approx c$, $\xi_3 \rightarrow -\infty$, $\xi_2 + \xi_3 \rightarrow -\infty$, and then Eq. (3.1) becomes $f \sim 1 + e^{\xi_1} + e^{\xi_3}$. This situation is the same as the case I (a) above.

(b) In the case of $t \rightarrow -\infty$, $y \rightarrow -\infty$: We have $\xi_3 \approx c$, $\xi_1 \rightarrow -\infty$, $\xi_3 \rightarrow +\infty$, $\xi_2 + \xi_3 \rightarrow +\infty$. and then Eq. (3.1) becomes

$$f \sim e^{\xi_3} + a_{23}e^{\xi_2 + \xi_3}, t \rightarrow -\infty, y \rightarrow -\infty.$$

Some of the asymptotic forms obtained above are repeated. After sorting, we get the asymptotic forms of the four arms as follows,

Before collision ($t \rightarrow -\infty$):

$$\begin{aligned} f_2^- &\sim 1 + e^{\eta_2}, f_3^- \sim 1 + a_{23}e^{\eta_3}, (y \rightarrow -\infty), \\ f_1 &\sim 1 + e^{\eta_1}, f_{1-2-3} \sim 1 + a_{23}e^{\eta_2+\eta_3-\eta_1}, (y \rightarrow +\infty). \end{aligned} \quad (3.3)$$

After collision ($t \rightarrow +\infty$):

$$\begin{aligned} f_2^+ &\sim 1 + a_{23}e^{\eta_2}, f_3^+ \sim 1 + e^{\eta_3}, (y \rightarrow -\infty), \\ f_1 &\sim 1 + e^{\eta_1}, f_{1-2-3} \sim 1 + a_{23}e^{\eta_2+\eta_3-\eta_1}, (y \rightarrow +\infty). \end{aligned} \quad (3.4)$$

Remark 3.1. Notations $^+$ and $^-$ are used to distinguish between f before and after the interaction. Comparing Eq. (3.3) and Eq. (3.4), f_j^+ and f_j^- differ by a phase shift at $t = \pm\infty$.

Remark 3.2. Eq. (3.2) is the exactly same as Eq. (3.3) for $t \rightarrow \infty$, which means that if we use the asymptotic analysis method in Ref. [19, 46–48] (consider t to be constant), we cannot get the asymptotic form (3.4) for $t \rightarrow +\infty$. The main difference between Eq. (3.3) and Eq. (3.4), as we have mentioned below Eq. (3.2), is due to the different appearance of phase shift term a_{23} , although both of them have four soliton arms.

Further, we can get the following proposition,

Proposition 3.1. The asymptotic forms of the weak 2-resonant 3-soliton with $0 < k_1 = k_3 < k_2$, $p_1 = p_2 > p_3 > 0$ are as following:

Before collision ($t \rightarrow -\infty$):

$$\begin{aligned} y \rightarrow +\infty, S_1 : \quad & u_1 \approx -\frac{k_1 p_1}{2} \operatorname{sech}^2\left(\frac{\xi_1}{2}\right), v_1 \approx -\frac{k_1^2}{2} \operatorname{sech}^2\left(\frac{\xi_1}{2}\right), \\ S_{1-2-3} : \quad & \widehat{u_{1-2-3}} \approx -\frac{(k_1 - k_2 - k_3)(p_1 - p_2 - p_3)}{2} \operatorname{sech}^2\left(\frac{\xi_1 - \xi_2 - \xi_3 - \ln a_{23}}{2}\right), \\ & \widehat{v_{1-2-3}} \approx -\frac{(k_1 - k_2 - k_3)^2}{2} \operatorname{sech}^2\left(\frac{\xi_1 - \xi_2 - \xi_3 - \ln a_{23}}{2}\right). \\ y \rightarrow -\infty, S_2 : \quad & u_2 \approx -\frac{k_2 p_2}{2} \operatorname{sech}^2\left(\frac{\xi_2}{2}\right), v_2 \approx -\frac{k_2^2}{2} \operatorname{sech}^2\left(\frac{\xi_2}{2}\right), \\ S_3 : \quad & \widehat{u_3} \approx -\frac{k_3 p_3}{2} \operatorname{sech}^2\left(\frac{\xi_3 + \ln a_{23}}{2}\right), \widehat{v_3} \approx -\frac{k_3^2}{2} \operatorname{sech}^2\left(\frac{\xi_3}{2}\right). \end{aligned} \quad (3.5)$$

After collision ($t \rightarrow +\infty$):

$$\begin{aligned} y \rightarrow +\infty, S_1 : \quad & u_1 \approx -\frac{k_1 p_1}{2} \operatorname{sech}^2\left(\frac{\xi_1}{2}\right), v_1 \approx -\frac{k_1^2}{2} \operatorname{sech}^2\left(\frac{\xi_1}{2}\right), \\ S_{1-2-3} : \quad & \widehat{u_{1-2-3}} \approx -\frac{(k_1 - k_2 - k_3)(p_1 - p_2 - p_3)}{2} \operatorname{sech}^2\left(\frac{\xi_1 - \xi_2 - \xi_3 - \ln a_{23}}{2}\right), \\ & \widehat{v_{1-2-3}} \approx -\frac{(k_1 - k_2 - k_3)^2}{2} \operatorname{sech}^2\left(\frac{\xi_1 - \xi_2 - \xi_3 - \ln a_{23}}{2}\right). \\ y \rightarrow -\infty, S_2 : \quad & \widehat{u_2} \approx -\frac{k_2 p_2}{2} \operatorname{sech}^2\left(\frac{\xi_2 + \ln a_{23}}{2}\right), \widehat{v_2} \approx -\frac{k_2^2}{2} \operatorname{sech}^2\left(\frac{\xi_2}{2}\right), \\ S_3 : \quad & u_3 \approx -\frac{k_3 p_3}{2} \operatorname{sech}^2\left(\frac{\xi_3}{2}\right), v_3 \approx -\frac{k_3^2}{2} \operatorname{sech}^2\left(\frac{\xi_3}{2}\right). \end{aligned} \quad (3.6)$$

Remark 3.3. In this paper, S_j corresponds to the soliton arms determined by f_j^- , f_j^+ and f_j . In contrast with Proposition 3.1, we find that analyzing the asymptotic form along the region $\zeta_j = x + \frac{p_j}{k_j}y = \text{constant}$ while considering t as a constant yields incomplete results (see Eq. (3.2)). Therefore, in this paper, we utilize the same method as Proposition 3.1 for our analysis.

Remark 3.4. To get the asymptotic forms (3.5) and (3.6), we need to make sure that $k_2p_3 - k_3p_2 > 0$. The same is true of the asymptotic forms (3.14) and (3.15) in section 3.3.

Remark 3.5. It can be seen from (3.5) and (3.6) that the asymptotic forms of the four arms are partially changed to t : The asymptotic form of S_2 and S_3 differ by a phase shift $\ln a_{23}$ at $t \rightarrow -\infty$ and $t \rightarrow +\infty$. If $a_{23} = 1$, the asymptotic forms (3.5) and (3.6) are the same, and the four arms shift over time without a phase shift. The same is true of the asymptotic forms (3.14) and (3.15) in section 3.3.

Especially, there are a special asymptotic form $f \sim e^{\xi_1} + e^{\xi_3}$ with $t \rightarrow +\infty$, $x \rightarrow \pm\infty$. It is generated by the resonances between S_1 and S_3 . Simultaneously, S_{1-3} (corresponding to $f \sim e^{\xi_1} + e^{\xi_3}$) resonates with S_2 , leading to the emergence of S_{1-2-3} . Considering the combined effects of these two sets of resonances and the location of the four arms (S_1 , S_2 , S_3 and S_{1-2-3}), we find the arms S_{1-3} manifests as a spatially finite structure, which is the stem structure we will study in this paper. And then, we investigate the behaviour of the intermediate regions for $t \rightarrow -\infty$. The resonance between soliton S_1 and soliton S_2 produces S_{1-2} (corresponding to $f \sim e^{\xi_1} + e^{\xi_2}$); simultaneously, S_{1-2} resonates with S_3 , resulting in the S_{1-2-3} . Due to the combined effects of these two sets of resonances and considering the location of the four arms, we find the arms S_{1-3} manifests as a spatially finite structure. Then, the asymptotic forms of the stems are given by

$$f_{1-2} \sim e^{\eta_1} + e^{\eta_2}, t \rightarrow -\infty, \text{ and } f_{1-3} \sim e^{\eta_1} + e^{\eta_3}, t \rightarrow +\infty. \quad (3.7)$$

It reveals a distinctive feature of the weak 2-resonant 3-soliton: a completely different stem structure with variable length before and after collision ($t \rightarrow \pm\infty$). Naturally, we have the following proposition,

Proposition 3.2. The stem structures corresponding to asymptotic forms (3.5) and (3.6) are as follows:

$$\begin{aligned} S_{1-2} : u_{1-2} &\approx -\frac{(k_1 - k_2)(p_1 - p_2)}{2} \text{sech}^2\left(\frac{\xi_1 - \xi_2}{2}\right), v_{1-2} \approx -\frac{(k_1 - k_2)^2}{2} \text{sech}^2\left(\frac{\xi_1 - \xi_2}{2}\right), t \rightarrow -\infty. \\ S_{1-3} : u_{1-3} &\approx -\frac{(k_1 - k_3)(p_1 - p_3)}{2} \text{sech}^2\left(\frac{\xi_1 - \xi_3}{2}\right), v_{1-3} \approx -\frac{(k_1 - k_3)^2}{2} \text{sech}^2\left(\frac{\xi_1 - \xi_3}{2}\right), t \rightarrow +\infty. \end{aligned} \quad (3.8)$$

The asymptotic forms given by proposition 3.1 and 3.2 reveal that the 2-resonant 3-soliton has four arms and a stem structure, and its evolution with time is illustrated in Fig. 1. When $t \rightarrow -\infty$, the stem structure S_{1-2} connects two pairs of V-shape solitons (S_1 and S_2 , S_1 and S_{1-2-3}). As time evolves, the length of this stem structure gradually diminishes until it vanishes around $t = 0$. At this moment, the four arms (S_1 , S_2 , S_3 , S_{1-2-3}) intersect together, and the two pairs of V-shape solitons turn into S_1 and S_3 , S_2 and S_{1-2-3} . As time passes ($t \rightarrow +\infty$), a new stem structure S_{1-3} appears, gradually growing longer and connecting these two pairs of V-shape solitons. This phenomenon is called soliton reconnection.

3.2. The stem structure with $0 < k_1 = k_3 < k_2$, $p_1 = p_2 > p_3 > 0$

The trajectories, amplitudes, and velocities of the four arms and two stems are listed in Tables 1 and 2, where

$$\begin{aligned} l_1: \xi_1 = 0, \quad l_2: \xi_2 = 0, \quad l_3: \xi_3 = 0, \quad \widehat{l}_2: \xi_2 + \ln a_{23} = 0, \quad \widehat{l}_3: \xi_3 + \ln a_{23} = 0, \\ l_{1-2}: \xi_1 - \xi_2 = 0, \quad l_{1-3}: \xi_1 - \xi_3 = 0, \quad \widehat{l_{1-2-3}}: \xi_1 - \xi_2 - \xi_3 - \ln a_{23} = 0. \end{aligned} \quad (3.9)$$

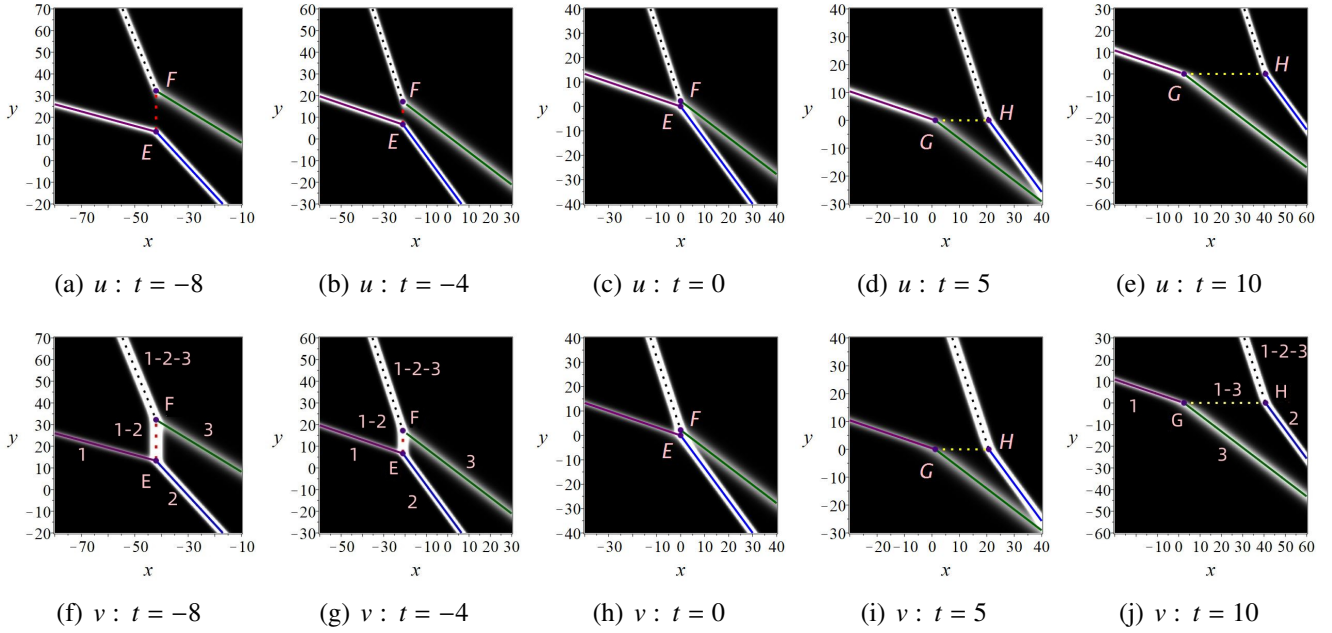


Figure 1: The density plots of the weak 2-resonant 3-soliton given by (2.1) and (3.1) with $k_1 = \frac{1}{2}$, $k_2 = 2$, $k_3 = \frac{1}{2}$, $p_1 = \frac{3}{2}$, $p_2 = \frac{3}{2}$, $p_3 = \frac{2}{3}$, $\xi_1^0 = 0$, $\xi_2^0 = 0$, $\xi_3^0 = 0$. The lines are the trajectories of the arms and stem structures, and the points are the endpoints of the variable length stem structures.

Here, \widehat{l}_j means that the formula of the trajectory contains a_{23} , otherwise not included, and its corresponding asymptotic form is \widehat{u}_j and \widehat{v}_j .

It's not hard to prove that the trajectories of S_1, S_2, S_{1-2} intersects at a point, and that the trajectories of S_3, S_{1-2-3}, S_{1-2} intersect at a point at $t \rightarrow -\infty$. In the same way, the trajectories of S_1, S_3, S_{1-3} intersects at a point, and that the trajectories of S_2, S_{1-2-3}, S_{1-3} intersect at a point at $t \rightarrow +\infty$. This further confirmed the correctness of the location of the stem structures (3.8). Notably, the amplitudes of $v_{1-2}, u_{1-2}, u_{1-3}$ all equal zero, implying that u effectively exhibits only four arms and a degenerated stem structure. It can be observed that l_{1-2} is oriented vertically, while l_{1-3} is oriented horizontally. Consequently, when $t \rightarrow -\infty$, the vertical variable length stem structure S_{1-2} , generated by resonance, gradually diminishes with time increase in length until it dissipates around $t = 0$. The resulting horizontal soliton exhibits an amplitude of zero. Interestingly, the trajectories and velocities of u and v are the same. Fig. 1 illustrates the trajectories of u and v at various moments, with the background representing the density plot. By solving for the intersection points of these trajectories, one can ascertain the endpoints of the variable-length stem structures as follows,

$$\begin{aligned}
 E & \left((k_1^2 + k_1 k_2 + k_2^2)t - \frac{\xi_1^0 - \xi_2^0}{k_1 - k_2}, -\frac{k_1 k_2 (k_1 + k_2)t}{p_1} + \frac{k_2 \xi_1^0 - k_1 \xi_2^0}{p_1 (k_1 - k_2)} \right), \\
 F & \left((k_1^2 + k_1 k_2 + k_2^2)t - \frac{\xi_1^0 - \xi_2^0}{k_1 - k_2}, -\frac{k_1 k_2 (k_1 + k_2)t + \ln a_{23} + \xi_3^0}{p_3} + \frac{k_1 (\xi_1^0 - \xi_2^0)}{p_3 (k_1 - k_2)} \right), \\
 G & \left(k_1^2 t - \frac{p_1 \xi_3^0 - p_3 \xi_1^0}{k_1 (p_1 - p_3)}, -\frac{\xi_1^0 - \xi_3^0}{p_1 - p_3} \right), H \left(k_2^2 t - \frac{\ln a_{23}}{k_2} + \frac{p_1 (\xi_1^0 - \xi_2^0 - \xi_3^0) + p_3 \xi_2^0}{k_2 (p_1 - p_3)}, -\frac{\xi_1^0 - \xi_3^0}{p_1 - p_3} \right).
 \end{aligned} \tag{3.10}$$

In this context, the point E corresponds to the intersection of lines l_1 and l_2 , while point F designates the intersection of lines \widehat{l}_3 and \widehat{l}_{1-2-3} . Point G marks the intersection of lines l_1 and l_3 , and point H denotes the intersection of lines \widehat{l}_2 and \widehat{l}_{1-2-3} , respectively. These points are also shown in Fig. 1. Whereupon, the

Table 2: Physical quantities of the arms with $0 < k_1 = k_3 < k_2$, $p_1 = p_2 > p_3 > 0$

Soliton	Trajectory	Velocity	Amplitude	Components
S_{1-2}	l_{1-2}	$(k_1^2 + k_1 k_2 + k_2^2, 0)$	$\begin{matrix} 0 \\ -\frac{(k_1-k_2)^2}{2} \end{matrix}$	$\begin{matrix} u_{1-2} \\ v_{1-2} \end{matrix}$
S_{1-3}	l_{1-3}	$(0, 0)$	$\begin{matrix} 0 \\ 0 \end{matrix}$	$\begin{matrix} u_{1-3} \\ v_{1-3} \end{matrix}$
S_{1-2-3}	$\widehat{l_{1-2-3}}$	$(k_2^2, -\frac{k_2^3}{p_3})$	$\begin{matrix} \frac{k_2 p_3}{2} \\ -\frac{k_2^2}{2} \end{matrix}$	$\begin{matrix} \widehat{u_{1-2-3}} \\ \widehat{v_{1-2-3}} \end{matrix}$

The solitons S_j ($j = 1-2, 1-3, 1-2-3$) are composed by two components u_j and v_j , and their trajectories are listed by (3.9).

lengths of the trajectories of the variable length stem structures are obtained as follows,

$$\begin{aligned} |EF| &= \left| \frac{k_1 k_2 (p_1 - p_3) (k_1^2 - k_2^2) t + p_1 (k_1 - k_2) \ln a_{23} - k_1 p_1 (\xi_1^0 - \xi_2^0 - \xi_3^0) - k_1 p_3 \xi_2^0 - k_2 p_1 \xi_3^0 + k_2 p_3 \xi_1^0}{p_1 p_3 (k_1 - k_2)} \right|, \\ |GH| &= \left| \frac{k_1 k_2 (p_1 - p_3) (k_1^2 - k_2^2) t + k_1 (p_1 - p_3) \ln a_{23} - k_1 p_1 (\xi_1^0 - \xi_2^0 - \xi_3^0) - k_1 p_3 \xi_2^0 - k_2 p_1 \xi_3^0 + k_2 p_3 \xi_1^0}{k_1 k_2 (p_1 - p_3)} \right|. \end{aligned} \quad (3.11)$$

Remark 3.6. Given the intricate complexity of the evolution around $t = 0$, the validity of the Eqs. (3.10) and (3.11) is constrained to scenarios where $t \ll 0$ and $t \gg 0$. This constraint equally applies to the subsequent Eqs. (3.17) and (3.18).

Now we will analyze the amplitudes of variable length stem structures next. Since the correlation analysis methods for u and v are identical, we only analyze v here. Below, we present only the formulas related to v , and the formulas for u are provided in the appendix. For computational convenience, we set $k_1 = \frac{1}{2}$, $k_2 = 2$, $k_3 = \frac{1}{2}$, $p_1 = \frac{3}{2}$, $p_2 = \frac{3}{2}$, $p_3 = \frac{2}{3}$, $\xi_1^0 = 0$, $\xi_2^0 = 0$, $\xi_3^0 = 0$. The cross-sectional curves of 3-soliton (2.1) with Eqs. (3.1) along l_{1-2} and l_{1-3} shown in Fig. 2 (a) and (b) are expressed as,

$$\begin{aligned} v|_{l_{1-2}}^{(1)} &= -\frac{13}{2} \cdot \frac{51e^{\frac{15t}{2} + \frac{11y}{3}} + 48e^{\frac{15t}{2} + \frac{17y}{6}} + 117e^{5t+3y} + 192e^{5t+\frac{13y}{6}} + 221e^{\frac{5t}{2} + \frac{3y}{2}} + 13e^{\frac{5t}{2} + \frac{2y}{3}}}{(3e^{5t+\frac{13y}{6}} + 26e^{\frac{5t}{2} + \frac{3y}{2}} + 13e^{\frac{5t}{2} + \frac{2y}{3}} + 13)^2}, \\ v|_{l_{1-3}}^{(1)} &= -\frac{13}{2} \cdot \frac{96e^{3x-\frac{33t}{4}} + 3e^{\frac{9x}{2} - \frac{129t}{8}} + 309e^{\frac{5x}{2} - \frac{65t}{8}} + 26e^{\frac{x}{2} - \frac{t}{8}} + 208e^{2x-8t}}{(3e^{\frac{5x}{2} - \frac{65t}{8}} + 26e^{\frac{x}{2} - \frac{t}{8}} + 13e^{2x-8t} + 13)^2}. \end{aligned} \quad (3.12)$$

Due to the intricacy of the calculations, providing explicit expressions for the extreme points along l_{1-2} and l_{1-3} is difficult. To approximate the amplitude of the variable length stem structures, we focus on the amplitudes at the midpoint of EF and GH , which are denoted as R_3 and R_4 respectively, to approximate the amplitudes of S_{1-2} and S_{1-3} . In instances where $|t| \gg 0$, the amplitudes of both u_{1-2} and u_{1-3} are rendered as zero. Consequently, we exclusively present the amplitude trend plot for component u in Fig. 3, while for component v , we provide both the amplitude formula and the corresponding trend plot across time. The amplitudes of S_{1-2} and S_{1-3} are expressed as:

$$\begin{aligned} S_{1-2} : v(R_1) &= -\frac{208\alpha_1 e^{\frac{425t}{144}} + 221\alpha_1 e^{\frac{25t}{16}} + 192\alpha_5 e^{\frac{325t}{144}} + 221\alpha_2 e^{\frac{25t}{36}} + 3e^{\frac{275t}{72}} - 507\alpha_2}{2\sqrt{39}(\alpha_3 e^{\frac{425t}{144}} + e^{\frac{325t}{144}} + \frac{3}{\sqrt{39}}e^{\frac{25t}{16}} + \frac{26\alpha_1}{3})^2}, \\ S_{1-3} : v(R_2) &= -\frac{3744\alpha_2 e^{\frac{45t}{8}} + 1205\alpha_4 e^{\frac{75t}{16}} + 8112e^{\frac{15t}{4}} + 1014\alpha_1 e^{\frac{135t}{16}} + 507\alpha_1 e^{\frac{15t}{16}}}{2\sqrt{39}(26\alpha_1 e^{\frac{75t}{16}} + 3\alpha_4 e^{\frac{15t}{16}} + \sqrt{39}e^{\frac{15}{4}} + 13)^2}, \end{aligned} \quad (3.13)$$

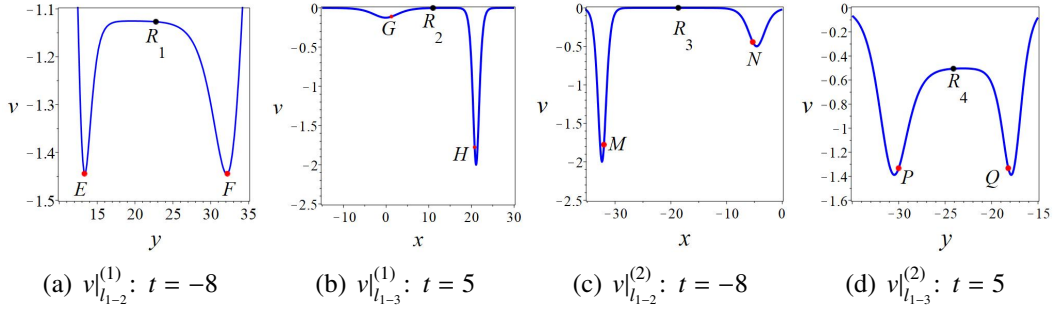


Figure 2: (a) (b) The cross-sectional curves (3.12); (c) (d) The cross-sectional curves (3.19). The red points are the endpoints of the variable length stem structures.

where $\alpha_1 = \left(\frac{3}{13}\right)^{\frac{3}{8}}$, $\alpha_2 = \left(\frac{13}{3}\right)^{\frac{1}{4}}$, $\alpha_3 = \left(\frac{3}{13}\right)^{\frac{1}{8}}$, $\alpha_4 = \left(\frac{13}{3}\right)^{\frac{1}{8}}$, $\alpha_5 = \sqrt[8]{39}$.
Just check out the limits:

$$\lim_{t \rightarrow +\infty} v(R_1) = 0, \quad \lim_{t \rightarrow -\infty} v(R_1) = 0, \quad \lim_{t \rightarrow +\infty} v(R_2) = -\frac{9}{8}, \quad \lim_{t \rightarrow -\infty} v(R_2) = 0.$$

You can also see this in Fig. 3. The amplitudes change with time are shown in Fig. 3 (c). As can be seen from the figure that S_{1-2} disappears and S_{1-3} arises around $t = 0$.

Remark 3.7. In this section, R_j is the midpoint of the variable length stem structures. Because the exact amplitude (the extreme value of the amplitude of the variable length stem structure) is difficult to solve analytically, we use $v(R_j)$ as the approximate amplitude of the variable length stem structure.

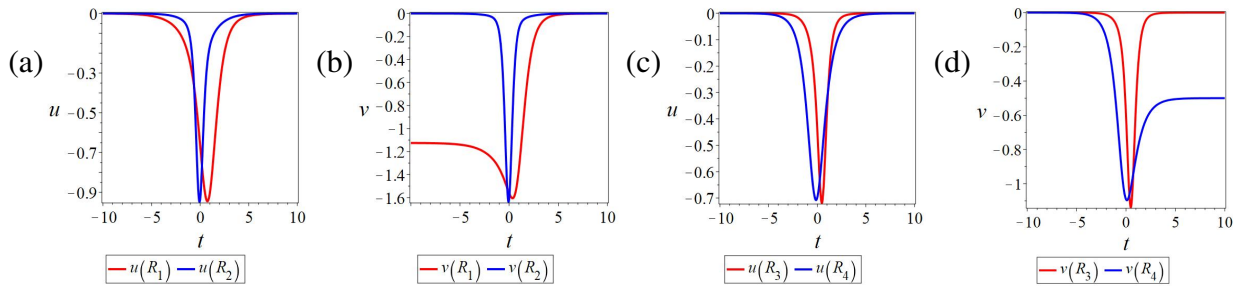


Figure 3: The evolutions of the amputation on the point R_j over time: (a)–(d) correspond to (5.2) (3.13) (5.4)(3.20), respectively.

3.3. The asymptotic analysis and stem structures with $k_1 = k_2 > k_3 > 0$, $0 < p_1 = p_3 < p_2$

Using the same method as in the section 3.1, the following propositions can be obtained.

Proposition 3.3. The asymptotic forms of the weak 2-resonant 3-soliton with $k_1 = k_2 > k_3 > 0$, $0 < p_1 = p_3 < p_2$ are as following:

Before collision ($t \rightarrow -\infty$):

$$\begin{aligned}
y \rightarrow -\infty, S_1 : \quad & u_1 \approx -\frac{k_1 p_1}{2} \operatorname{sech}^2\left(\frac{\xi_1}{2}\right), \quad v_1 \approx -\frac{k_1^2}{2} \operatorname{sech}^2\left(\frac{\xi_1}{2}\right), \\
S_{1-2-3} : \quad & \widehat{u_{1-2-3}} \approx -\frac{(k_1 - k_2 - k_3)(p_1 - p_2 - p_3)}{2} \operatorname{sech}^2\left(\frac{\xi_1 - \xi_2 - \xi_3 - \ln a_{23}}{2}\right), \\
& \widehat{v_{1-2-3}} \approx -\frac{(k_1 - k_2 - k_3)^2}{2} \operatorname{sech}^2\left(\frac{\xi_1 - \xi_2 - \xi_3 - \ln a_{23}}{2}\right), \\
y \rightarrow +\infty, S_2 : \quad & u_2 \approx -\frac{k_2 p_2}{2} \operatorname{sech}^2\left(\frac{\xi_2}{2}\right), \quad v_2 \approx -\frac{k_2^2}{2} \operatorname{sech}^2\left(\frac{\xi_2}{2}\right), \\
S_3 : \quad & \widehat{u_3} \approx -\frac{k_3 p_3}{2} \operatorname{sech}^2\left(\frac{\xi_3 + \ln a_{23}}{2}\right), \quad \widehat{v_3} \approx -\frac{k_3^2}{2} \operatorname{sech}^2\left(\frac{\xi_3}{2}\right).
\end{aligned} \tag{3.14}$$

After collision ($t \rightarrow +\infty$):

$$\begin{aligned}
y \rightarrow -\infty, S_1 : \quad & u_1 \approx -\frac{k_1 p_1}{2} \operatorname{sech}^2\left(\frac{\xi_1}{2}\right), \quad v_1 \approx -\frac{k_1^2}{2} \operatorname{sech}^2\left(\frac{\xi_1}{2}\right), \\
S_{1-2-3} : \quad & \widehat{u_{1-2-3}} \approx -\frac{(k_1 - k_2 - k_3)(p_1 - p_2 - p_3)}{2} \operatorname{sech}^2\left(\frac{\xi_1 - \xi_2 - \xi_3 - \ln a_{23}}{2}\right), \\
& \widehat{v_{1-2-3}} \approx -\frac{(k_1 - k_2 - k_3)^2}{2} \operatorname{sech}^2\left(\frac{\xi_1 - \xi_2 - \xi_3 - \ln a_{23}}{2}\right), \\
y \rightarrow +\infty, S_2 : \quad & \widehat{u_2} \approx -\frac{k_2 p_2}{2} \operatorname{sech}^2\left(\frac{\xi_2 + \ln a_{23}}{2}\right), \quad \widehat{v_2} \approx -\frac{k_2^2}{2} \operatorname{sech}^2\left(\frac{\xi_2}{2}\right), \\
S_3 : \quad & u_3 \approx -\frac{k_3 p_3}{2} \operatorname{sech}^2\left(\frac{\xi_3}{2}\right), \quad v_3 \approx -\frac{k_3^2}{2} \operatorname{sech}^2\left(\frac{\xi_3}{2}\right).
\end{aligned} \tag{3.15}$$

Proposition 3.4. *The stem structures corresponding to asymptotic forms (3.14) and (3.15) are as following:*

$$\begin{aligned}
S_{1-2} : \quad & u_{1-2} \approx -\frac{(k_1 - k_2)(p_1 - p_2)}{2} \operatorname{sech}^2\left(\frac{\xi_1 - \xi_2}{2}\right), \quad v_{1-2} \approx -\frac{(k_1 - k_2)^2}{2} \operatorname{sech}^2\left(\frac{\xi_1 - \xi_2}{2}\right), \quad t \rightarrow -\infty. \\
S_{1-3} : \quad & u_{1-3} \approx -\frac{(k_1 - k_3)(p_1 - p_3)}{2} \operatorname{sech}^2\left(\frac{\xi_1 - \xi_3}{2}\right), \quad v_{1-3} \approx -\frac{(k_1 - k_3)^2}{2} \operatorname{sech}^2\left(\frac{\xi_1 - \xi_3}{2}\right), \quad t \rightarrow +\infty.
\end{aligned} \tag{3.16}$$

Comparing the proposition 3.1–3.4, we find that the asymptotic forms of four arms in two cases have a coordinates translation, and the asymptotic forms of stem structures are the same. Therefore, the dynamical evolutions of solitons in these two cases are also very similar, as illustrated in Fig. 4. Next, we analyse the properties of stem structures.

The trajectories, amplitudes, and velocities of the arms are outlined in Tables 1 and 3. In this case, the amplitude of u_{1-2} and u_{1-3} are zero, while the amplitude of v_{1-2} and v_{1-3} respectively are zero and $-\frac{(k_1 - k_3)^2}{2}$. And the lines are the trajectories at different moments. It can be seen from the above analysis and figures that when $t \rightarrow -\infty$, the horizontal variable length stem S_{1-2} produced by the resonance gradually decreases in length until it disappears around $t = 0$, and the resulting vertical variable length stem S_{1-3} when $t \rightarrow +\infty$. By solving the intersection points of trajectories, the endpoints of the variable-length stem

Table 3: Physical quantities of the arms with $k_1 = k_2 > k_3 > 0$, $0 < p_1 = p_3 < p_2$

Soliton	Trajectory	Velocity	Amplitude	Components
S_{1-2}	l_{1-2}	$(0, 0)$	0	u_{1-2}
			0	v_{1-2}
S_{1-3}	l_{1-3}	$(k_1^2 + k_1 k_3 + k_3^2, 0)$	0	u_{1-3}
			$-\frac{(k_1 - k_3)^2}{2}$	v_{1-3}
S_{1-2-3}	$\widehat{l_{1-2-3}}$	$(k_3^2, -\frac{k_3^3}{p_2})$	$\frac{k_3 p_2}{2}$	$\widehat{u_{1-2-3}}$
			$-\frac{k_3^2}{2}$	$\widehat{v_{1-2-3}}$

The solitons S_j ($j = 1-2, 1-3, 1-2-3$) are composed by two components u_j and v_j , and their trajectories are listed by (3.9).

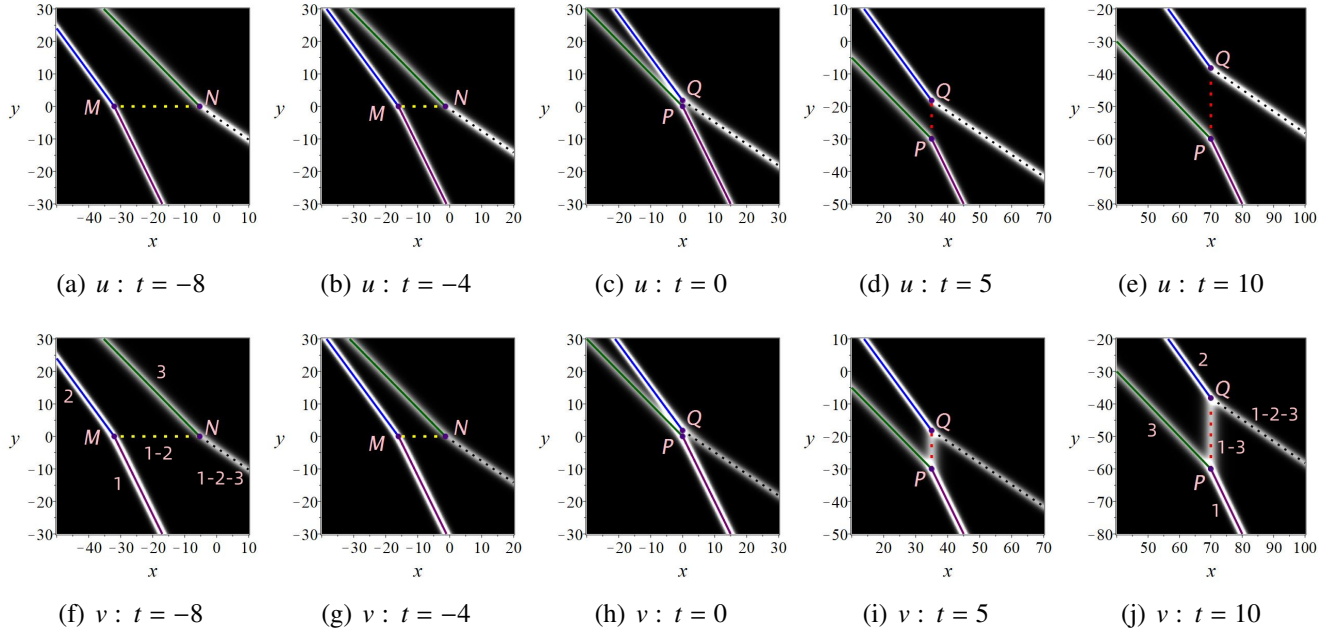


Figure 4: The density plots of the weak 2-resonant 3-soliton given by (2.1) and (3.1) with $k_1 = 2$, $k_2 = 2$, $k_3 = 1$, $p_1 = 1$, $p_2 = \frac{3}{2}$, $p_3 = 1$, $\xi_1^0 = 0$, $\xi_2^0 = 0$, $\xi_3^0 = 0$. The lines are the trajectories of the arms and stem structures, and the points are the endpoints of the variable length stem structures.

structures can be obtained as

$$\begin{aligned}
 &M \left(k_1^2 t - \frac{p_1 \xi_2^0 - p_2 \xi_1^0}{k_1(p_1 - p_2)}, -\frac{\xi_1^0 - \xi_2^0}{p_1 - p_2} \right), N \left(-k_3^2 t + \frac{\ln a_{23}}{k_3} - \frac{p_1(\xi_1^0 - \xi_2^0 - \xi_3^0) + p_2 \xi_3^0}{k_3(p_1 - p_2)}, -\frac{\xi_1^0 - \xi_3^0}{p_1 - p_2} \right), \\
 &P \left((k_1^2 + k_1 k_3 + k_3^2)t - \frac{\xi_1^0 - \xi_3^0}{k_1 - k_3}, -\frac{k_1 k_3(k_1 + k_3)t}{p_1} + \frac{k_3 \xi_1^0 - k_1 \xi_3^0}{p_1(k_1 - k_3)} \right), \\
 &Q \left((k_1^2 + k_1 k_3 + k_3^2)t - \frac{\xi_1^0 - \xi_3^0}{k_1 - k_3}, -\frac{k_1 k_3(k_1 + k_3)t + \ln a_{23} + \xi_2^0}{p_2} + \frac{k_1(\xi_1^0 - \xi_3^0)}{p_2(k_1 - k_3)} \right).
 \end{aligned} \tag{3.17}$$

Here, “M” and “N” represent the intersections of l_1 and l_2 , $\widehat{l_3}$ and $\widehat{l_{1-2-3}}$ at $t \ll 0$, while “P” and “Q” denote the intersections of l_1 and l_3 , $\widehat{l_2}$ and $\widehat{l_{1-2-3}}$ at $t \gg 0$. These specific points are visually illustrated in Fig. 4. Subsequently, the lengths of the trajectories of the variable length stem structures are determined as

follows:

$$\begin{aligned} |PQ| &= \left| \frac{k_1 k_3 (p_1 - p_2)(k_1^2 - k_3^2)t + p_1(k_1 - k_3) \ln a_{23} - k_1 p_1 (\xi_1^0 - \xi_2^0 - \xi_3^0) - k_1 p_2 \xi_3^0 - k_3 p_1 \xi_2^0 + k_3 p_2 \xi_1^0}{p_1 p_2 (k_1 - k_3)} \right|, \\ |MN| &= \left| \frac{k_1 k_3 (p_1 - p_2)(k_1^2 - k_3^2)t + k_1(p_1 - p_2) \ln a_{23} - k_1 p_1 (\xi_1^0 - \xi_2^0 - \xi_3^0) - k_1 p_2 \xi_3^0 - k_3 p_1 \xi_2^0 + k_3 p_2 \xi_1^0}{k_1 k_3 (p_1 - p_2)} \right|. \end{aligned} \quad (3.18)$$

Now, we analyze the amplitudes of variable length stem structures. Here we direct our attention to v , and the formula for u corresponding to Eqs. (3.19) and (3.20) are provided in the appendix. To simplify the calculation, we choose $k_1 = 2$, $k_2 = 2$, $k_3 = 1$, $p_1 = 1$, $p_2 = \frac{3}{2}$, $p_3 = 1$, $\xi_1^0 = 0$, $\xi_2^0 = 0$, $\xi_3^0 = 0$. The cross-sectional curves of 3-soliton (2.1) with Eqs. (3.1) along l_{1-2} and l_{1-3} shown in Fig. 2 (c) and (d) are expressed as,

$$\begin{aligned} v|_{l_{1-2}}^{(2)} &= -\frac{30(2e^{5x-17t} + 4e^{4x-10t} + 39e^{3x-9t} + 120e^{2x-8t} + 15e^{x-t})}{(e^{3x-9t} + 30e^{2x-8t} + 15e^{x-t} + 15)^2}, \\ v|_{l_{1-3}}^{(2)} &= -\frac{30(5e^{\frac{7y}{2}+18t} + e^{4y+18t} + 15e^{2y+12t} + 24e^{\frac{5y}{2}+12t} + 75e^{y+6t} + 60e^{\frac{3y}{2}+6t})}{(e^{\frac{5y}{2}+12t} + 30e^{y+6t} + 15e^{\frac{3y}{2}+6t} + 15)^2}. \end{aligned} \quad (3.19)$$

Since the extreme points and values are difficult to express explicitly, we study the amplitude at the midpoint of MN and PQ , denoted by R_3 and R_4 . Similar to the preceding case in this section, we exclusively showcase the amplitude trend plot for component u in Fig. 3. Conversely, for component v , we furnish the amplitude formula and the associated trend plot over time. Then, the amplitudes of the variable length stem structures, respectively, are

$$\begin{aligned} S_{1-2} : \quad v(R_3) &= -\frac{\alpha_6 \left(2e^{\frac{15t}{2}} + 30e^{\frac{9t}{2}} + 6\alpha_6 e^{6t} + 10\alpha_6 e^{3t} + 75 \right)}{\left(\alpha_6 e^{\frac{9t}{2}} + \alpha_6 e^{\frac{3t}{2}} + e^{3t} + 30 \right)^2}, \\ S_{1-3} : \quad v(R_4) &= -\frac{225 \cdot \left(2\alpha_6 \alpha_7 e^{\frac{5t}{2}} + 6\alpha_7 e^{4t} + 9\alpha_8 e^{\frac{7t}{2}} + 6\alpha_6 e^{\frac{3t}{2}} + 2\alpha_7 e^t \right)}{\left(\alpha_6 \alpha_7 e^t + 30\alpha_7 e^{\frac{5t}{2}} + 15e^{\frac{3t}{2}} + 15\sqrt{15} \right)^2}, \end{aligned} \quad (3.20)$$

where $\alpha_6 = \sqrt{15}$, $\alpha_7 = \sqrt[3]{15}$, $\alpha_8 = \sqrt[6]{15}$.

The limits are easily obtained:

$$\lim_{t \rightarrow +\infty} v(R_3) = 0, \quad \lim_{t \rightarrow -\infty} v(R_3) = 0, \quad \lim_{t \rightarrow +\infty} v(R_4) = -\frac{1}{2}, \quad \lim_{t \rightarrow -\infty} v(R_4) = 0.$$

These results align with the observations in Fig. 3. The figures of (3.20) are shown in Fig. 3 (b). As can be seen from the figure that S_{1-2} disappears around $t = 0$, and S_{1-3} arises.

4. The stem structure in 3-soliton generated by strong 2-resonance in soliton reconnection

In this section, we shall use two-variable asymptotic method to study the 3-soliton with strong 2-resonance. By substituting $\xi_2^0 \rightarrow \xi_2^0 - \ln a_{12}$ and $\xi_3^0 \rightarrow \xi_3^0 - \ln a_{13}$ (equivalent to $\xi_2 \rightarrow \xi_2 - \ln a_{12}$ and $\xi_3 \rightarrow \xi_3 - \ln a_{13}$) into Eq. (2.4) and taking the limit as $a_{12}, a_{13} \rightarrow \infty$, we can derive

$$f_{strong} = 1 + \exp \xi_1 + \exp(\xi_1 + \xi_2) + \exp(\xi_1 + \xi_3) + a_{23} \exp(\xi_1 + \xi_2 + \xi_3). \quad (4.1)$$

The 3-soliton with strong 2-resonance is precisely described by Eqs. (4.1) and (2.1). To ensure that $a_{12} = \infty$, $a_{13} = \infty$, and $0 < a_{23} < +\infty$, two distinct cases emerge: (i) $0 < k_1 = -k_3 < k_2$, $p_1 = -p_2 > p_3 > 0$; (ii) $k_1 = -k_2 > k_3 > 0$, $0 < p_1 = -p_3 < p_2$. Next, we will analyze these two cases separately.

Table 4: Physical quantities of the arms with $0 < k_1 = -k_3 < k_2$, $p_1 = -p_2 > p_3 > 0$

Soliton	Trajectory	Velocity	Amplitude	Components
S_{1+2}	l_{1+2}	$(k_1^2 - k_1k_2 + k_2^2, 0)$	$\begin{matrix} 0 \\ -\frac{(k_1+k_2)^2}{2} \end{matrix}$	$\begin{matrix} u_{1+2} \\ v_{1+2} \end{matrix}$
S_{1+3}	l_{1+3}	$(0, 0)$	$\begin{matrix} 0 \\ 0 \end{matrix}$	$\begin{matrix} u_{1+3} \\ v_{1+3} \end{matrix}$
S_{1+2+3}	$\widehat{l_{1+2+3}}$	$(k_2^2, -\frac{k_2^3}{p_3})$	$\begin{matrix} \frac{k_2p_3}{2} \\ -\frac{k_2^2}{2} \end{matrix}$	$\begin{matrix} \widehat{u_{1+2+3}} \\ \widehat{v_{1+2+3}} \end{matrix}$

The solitons S_j ($j = 1 + 2, 1 + 3, 1 + 2 + 3$) are composed by two components u_j and v_j , and their trajectories are listed by (4.7).

4.1. The asymptotic analysis with $0 < k_1 = -k_3 < k_2$, $p_1 = -p_2 > p_3 > 0$

First we use a similar method to the previous section for asymptotic analysis.

I. On the region $\eta_1 = x + \frac{p_1}{k_1}y - k_1^2t$, we have

$$\begin{aligned} \xi_1 &= k_1\eta_1 + c_1, \quad \xi_1 + \xi_2 = (k_1 + k_2)\eta_1 + \frac{k_1p_2 - k_2p_1}{k_1}y + k_2(k_1^2 - k_2^2)t + c_2, \\ \xi_1 + \xi_3 &= (k_1 + k_3)\eta_1 + \frac{k_1p_3 - k_3p_1}{k_1}y + c_3, \\ \xi_1 + \xi_2 + \xi_3 &= (k_1 + k_2 + k_3)\eta_1 + \frac{(p_2 + p_3)k_1 - p_1(k_2 + k_3)}{k_1}y + ((k_2 + k_3)k_1^2 - (k_2^3 + k_3^3))t + c_4. \end{aligned}$$

(a) In the case of $t \rightarrow +\infty$: We have $\xi_1 \approx c$, $\xi_1 + \xi_2 \rightarrow -\infty$, $\xi_1 + \xi_3 \approx c$, $\xi_1 + \xi_2 + \xi_3 \rightarrow -\infty$, and then $f \sim 1 + e^{\xi_1} + e^{\xi_1+\xi_3}$. Further we can get:

$$f \sim 1 + e^{\xi_1}, \quad y \rightarrow -\infty; \quad f \sim e^{\xi_1} + e^{\xi_1+\xi_3}, \quad y \rightarrow +\infty; \quad f \sim 1 + e^{\xi_1+\xi_3}, \quad x \rightarrow -\infty.$$

(b) In the case of $t \rightarrow -\infty$: We have $\xi_1 \approx c$, $\xi_1 + \xi_2 \rightarrow +\infty$, $\xi_1 + \xi_3 \rightarrow -\infty$, $\xi_1 + \xi_2 + \xi_3 \rightarrow +\infty$, and then $f \sim e^{\xi_1+\xi_2} + a_{23}e^{\xi_1+\xi_2+\xi_3}$. It can only be determined if the arm appears at $t \rightarrow -\infty$, not whether it is on $y \rightarrow +\infty$ or $y \rightarrow -\infty$.

II. On the region $\eta_2 = x + \frac{p_2}{k_2}y - k_2^2t$, we have

$$\begin{aligned} \xi_1 &= k_1\eta_2 + \frac{k_2p_1 - k_1p_2}{k_2}y + k_1(k_2^2 - k_1^2)t + c_1, \\ \xi_1 + \xi_2 &= (k_1 + k_2)\eta_2 + \frac{k_2p_1 - k_1p_2}{k_2}y + k_1(k_2^2 - k_1^2)t + c_2, \\ \xi_1 + \xi_3 &= (k_1 + k_3)\eta_2 + (p_1 + p_3)y + k_2^2(k_1 + k_3)t + c_3, \\ \xi_1 + \xi_2 + \xi_3 &= (k_1 + k_2 + k_3)\eta_2 + (p_1 + p_3)y + k_2^2(k_1 + k_3)t + c_4. \end{aligned}$$

(a) In the case of $t \rightarrow -\infty$: We have $\xi_2 \approx c$, $\xi_1 \rightarrow -\infty$, $\xi_1 + \xi_2 \rightarrow -\infty$, $\xi_1 + \xi_3 \approx c$, $\xi_1 + \xi_2 + \xi_3 \approx c$, and then $f \sim 1 + e^{\xi_1+\xi_3} + a_{23}e^{\xi_1+\xi_2+\xi_3}$. Further we can get:

$$f \sim e^{\xi_1+\xi_3} + a_{23}e^{\xi_1+\xi_2+\xi_3}, \quad y \rightarrow +\infty; \quad f \sim 1 + a_{23}e^{\xi_1+\xi_2+\xi_3}, \quad y \rightarrow -\infty; \quad f \sim 1 + e^{\xi_1+\xi_3}, \quad x \rightarrow -\infty.$$

(b) In the case of $t \rightarrow +\infty$, $y \rightarrow +\infty$: By the limit $y \rightarrow +\infty$, we can get $\xi_2 \approx c$, $\xi_1 \rightarrow +\infty$, $\xi_1 + \xi_2 \rightarrow +\infty$, $\xi_1 + \xi_3 \rightarrow +\infty$, $\xi_1 + \xi_2 + \xi_3 \rightarrow +\infty$. So $f \sim e^{\xi_1} + e^{\xi_1+\xi_2} + e^{\xi_1+\xi_3} + a_{23}e^{\xi_1+\xi_2+\xi_3} = e^{\xi_1}(1 + e^{\xi_2} + e^{\xi_3} + a_{23}e^{\xi_2+\xi_3})$. Due to $\xi_3 \rightarrow -\infty$, it can be get as following

$$f \sim 1 + e^{\xi_2}, \quad t \rightarrow +\infty, \quad y \rightarrow +\infty.$$

III. On the region $\eta_3 = x + \frac{p_3}{k_3}y - k_3^2 t$, we have

$$\begin{aligned}\xi_1 &= k_1 \eta_3 + \frac{k_3 p_1 - k_1 p_3}{k_3} y + c_1, \\ \xi_1 + \xi_2 &= (k_1 + k_2) \eta_3 + \frac{k_2(p_1 + p_3)}{k_3} y + k_2(k_3^2 - k_2^2) t + c_2, \\ \xi_1 + \xi_3 &= (k_1 + k_3) \eta_3 + \frac{k_3 p_1 - k_1 p_3}{k_3} y + c_3, \\ \xi_1 + \xi_2 + \xi_3 &= (k_1 + k_2 + k_3) \eta_1 + \frac{k_2(p_1 + p_3)}{k_3} y + k_2(k_3^2 - k_2^2) t + c_4.\end{aligned}$$

(a) In the case of $t \rightarrow +\infty$: We have $\xi_3 \approx c$, $\xi_1 \approx c$, $\xi_1 + \xi_2 \rightarrow -\infty$, $\xi_1 + \xi_3 \approx c$, $\xi_1 + \xi_2 + \xi_3 \rightarrow -\infty$, and then $f \sim 1 + e^{\xi_1} + e^{\xi_1 + \xi_3}$. This situation is the same as the case **I (a)** above.

(b) In the case of $t \rightarrow -\infty$, $y \rightarrow +\infty$: We have $\xi_3 \approx c$, $\xi_1 \rightarrow +\infty$, $\xi_1 + \xi_2 \rightarrow +\infty$, $\xi_1 + \xi_3 \rightarrow +\infty$, $\xi_1 + \xi_2 + \xi_3 \rightarrow +\infty$. Because of $\xi_2 \gg \xi_3$ when $t \rightarrow -\infty$, so we have

$$f \sim e^{\xi_1 + \xi_2} + a_{23} e^{\xi_1 + \xi_2 + \xi_3}, \quad t \rightarrow -\infty, \quad y \rightarrow +\infty.$$

IV. On the region $\eta_4 = x + \frac{p_1 + p_2}{k_1 + k_2} y - (k_1^3 + k_2^2) t$, we have

$$\begin{aligned}\xi_1 &= k_1 \eta_3 + \frac{k_3 p_1 - k_1 p_3}{k_3} y + c_1, \\ \xi_1 + \xi_2 &= (k_1 + k_2) \eta_3 + \frac{k_2(p_1 + p_3)}{k_3} y + k_2(k_3^2 - k_2^2) t + c_2, \\ \xi_1 + \xi_3 &= (k_1 + k_3) \eta_3 + \frac{k_3 p_1 - k_1 p_3}{k_3} y + c_3, \\ \xi_1 + \xi_2 + \xi_3 &= (k_1 + k_2 + k_3) \eta_1 + \frac{k_2(p_1 + p_3)}{k_3} y + k_2(k_3^2 - k_2^2) t + c_4.\end{aligned}$$

(a) In the case of $y \rightarrow -\infty$: We have $\xi_1 \rightarrow -\infty$, $\xi_1 + \xi_2 \approx c$, $\xi_1 + \xi_3 \rightarrow -\infty$, $\xi_1 + \xi_2 + \xi_3 \rightarrow -\infty$, and then $f \sim 1 + e^{\xi_1 + \xi_2}$. Considering the analysis of cases **I–III** presented in this section, and noting that soliton S_{1+2} arises from a strong resonance between S_1 and S_2 ($a_{12} \rightarrow +\infty$), it is evident that there is no phase shift as $t \rightarrow -\infty$ or $t \rightarrow +\infty$. Hence, it can be inferred that this soliton persists indefinitely as $t \rightarrow \pm\infty$, namely,

$$f \sim 1 + e^{\xi_1 + \xi_2}, \quad y \rightarrow -\infty, \quad t \rightarrow \pm\infty.$$

We notice that some of the asymptotic forms obtained from the above analysis are repeated. After sorting, the asymptotic forms are as follows:

Before collision ($t \rightarrow -\infty$):

$$\begin{aligned}f_2^- &\sim 1 + a_{23} e^{\eta_2}, \quad f_3^- \sim 1 + a_{23} e^{\eta_3}, \quad (y \rightarrow +\infty), \\ f_{1+2} &\sim 1 + e^{\eta_1 + \eta_2}, \quad (y \rightarrow -\infty), \\ f_{1+3} &\sim 1 + e^{\eta_1 + \eta_3}, \quad (x \rightarrow -\infty).\end{aligned}\tag{4.2}$$

After collision ($t \rightarrow +\infty$):

$$\begin{aligned}f_2^+ &\sim 1 + e^{\eta_2}, \quad f_3^+ \sim 1 + e^{\eta_3}, \quad (y \rightarrow +\infty), \\ f_{1+2} &\sim 1 + e^{\eta_1 + \eta_2}, \quad (y \rightarrow -\infty), \\ f_{1+3} &\sim 1 + e^{\eta_1 + \eta_3}, \quad (x \rightarrow -\infty).\end{aligned}\tag{4.3}$$

Then we have the following proposition:

Proposition 4.1. *The asymptotic forms of the strong 2-resonant 3-soliton with $0 < k_1 = -k_3 < k_2$, $p_1 = -p_2 > p_3 > 0$ are as following:*

Before collision ($t \rightarrow -\infty$):

$$\begin{aligned}
x \rightarrow +\infty, S_2 : \quad \widehat{u}_2 &\approx -\frac{k_2 p_2}{2} \operatorname{sech}^2\left(\frac{\xi_2 + \ln a_{23}}{2}\right), \widehat{v}_2 \approx -\frac{k_2^2}{2} \operatorname{sech}^2\left(\frac{\xi_2}{2}\right), \\
S_3 : \quad \widehat{u}_3 &\approx -\frac{k_3 p_3}{2} \operatorname{sech}^2\left(\frac{\xi_3 + \ln a_{23}}{2}\right), \widehat{v}_3 \approx -\frac{k_3^2}{2} \operatorname{sech}^2\left(\frac{\xi_3 + \ln a_{23}}{2}\right), \\
x \rightarrow -\infty, S_{1+3} : \quad u_{1+3} &\approx -\frac{(k_1 + k_3)(p_1 + p_3)}{2} \operatorname{sech}^2\left(\frac{\xi_1 + \xi_3}{2}\right), v_{1+3} \approx -\frac{(k_1 + k_3)^2}{2} \operatorname{sech}^2\left(\frac{\xi_1 + \xi_3}{2}\right), \\
y \rightarrow -\infty, S_{1+2} : \quad u_{1+2} &\approx -\frac{(k_1 + k_2)(p_1 + p_2)}{2} \operatorname{sech}^2\left(\frac{\xi_1 + \xi_2}{2}\right), v_{1+2} \approx -\frac{(k_1 + k_2)^2}{2} \operatorname{sech}^2\left(\frac{\xi_1 + \xi_2}{2}\right).
\end{aligned} \tag{4.4}$$

After collision ($t \rightarrow +\infty$):

$$\begin{aligned}
x \rightarrow +\infty, S_2 : \quad u_2 &\approx -\frac{k_2 p_2}{2} \operatorname{sech}^2\left(\frac{\xi_2}{2}\right), v_2 \approx -\frac{k_2^2}{2} \operatorname{sech}^2\left(\frac{\xi_2}{2}\right), \\
S_3 : \quad u_3 &\approx -\frac{k_3 p_3}{2} \operatorname{sech}^2\left(\frac{\xi_3}{2}\right), v_3 \approx -\frac{k_3^2}{2} \operatorname{sech}^2\left(\frac{\xi_3}{2}\right). \\
x \rightarrow -\infty, S_{1+3} : \quad u_{1+3} &\approx -\frac{(k_1 + k_3)(p_1 + p_3)}{2} \operatorname{sech}^2\left(\frac{\xi_1 + \xi_3}{2}\right), v_{1+3} \approx -\frac{(k_1 + k_3)^2}{2} \operatorname{sech}^2\left(\frac{\xi_1 + \xi_3}{2}\right), \\
y \rightarrow -\infty, S_{1+2} : \quad u_{1+2} &\approx -\frac{(k_1 + k_2)(p_1 + p_2)}{2} \operatorname{sech}^2\left(\frac{\xi_1 + \xi_2}{2}\right), v_{1+2} \approx -\frac{(k_1 + k_2)^2}{2} \operatorname{sech}^2\left(\frac{\xi_1 + \xi_2}{2}\right).
\end{aligned} \tag{4.5}$$

Remark 4.1. *It can be seen from (4.4) and (4.5) that the asymptotic forms of the four arms are partially changed with respect to t : The asymptotic form of S_2 and S_3 differ by a phase shift $\ln a_{23}$ at $t \rightarrow -\infty$ and $t \rightarrow +\infty$. If $a_{23} = 1$, the asymptotic forms (4.4) and (4.5) are the same, and the four arms shift over time without a phase shift. The same is true of the asymptotic forms (4.12) and (4.13) in section 4.3.*

And then we consider the two special arms S_1 and S_{1+2+3} which respectively associated with $f \sim 1 + e^{\xi_1}$ ($t \rightarrow +\infty$) and $f \sim 1 + a_{23}e^{\xi_1 + \xi_2 + \xi_3}$ ($t \rightarrow -\infty$) in the asymptotic analysis above. When $t \rightarrow +\infty$, the resonance between S_1 and S_2 leads to the S_{1+2} , the resonance between S_1 and S_3 leads to the S_{1+3} . When $t \rightarrow -\infty$, the resonances between S_2 and S_{1+3} leads to the S_{1+2+3} which can also be viewed as generated by the resonance between S_3 and S_{1+2} . Considering the asymptotic trend of the four arms, we can see that S_1 and S_{1+2+3} actually local structures of finite length which named by stem structures in this paper. Then we have asymptotic forms of the stems as,

$$f_1 \sim 1 + e^{\xi_1}, t \rightarrow +\infty, \text{ and } f_{1+2+3} \sim 1 + a_{23}e^{\xi_1 + \xi_2 + \xi_3}, t \rightarrow -\infty.$$

Namely,

Proposition 4.2. *The stem structures corresponding to asymptotic forms (4.4) and (4.5) are as following:*

$$\begin{aligned}
t \rightarrow +\infty, S_1 : \quad u_1 &\approx -\frac{k_1 p_1}{2} \operatorname{sech}^2\left(\frac{\xi_1}{2}\right), v_1 \approx -\frac{k_1^2}{2} \operatorname{sech}^2\left(\frac{\xi_1}{2}\right), \\
t \rightarrow -\infty, S_{1+2+3} : \quad \widehat{u_{1+2+3}} &\approx -\frac{(k_1 + k_2 + k_3)(p_1 + p_2 + p_3)}{2} \operatorname{sech}^2\left(\frac{\xi_1 + \xi_2 + \xi_3 + \ln a_{23}}{2}\right), \\
\widehat{v_{1+2+3}} &\approx -\frac{(k_1 + k_2 + k_3)^2}{2} \operatorname{sech}^2\left(\frac{\xi_1 + \xi_2 + \xi_3}{2}\right).
\end{aligned} \tag{4.6}$$

According to proposition 4.1 and 4.2, the asymptotic forms indicate that the 2-resonant 3-soliton features a configuration with four arms and a central stem. This temporal evolution is depicted in Fig. 5. As $t \rightarrow -\infty$, the stem structure S_{1+2+3} links two pairs of V-shaped solitons: S_2 and S_{1+3} , S_3 and S_{1+2} . Over time, this stem structure shortens and eventually disappears around $t = 0$. At this critical moment, the four arms ($S_2, S_3, S_{1+2}, S_{1+3}$) converge, transforming the pairs of V-shaped solitons into S_2 and S_{1+2} , S_3 and S_{1+3} . As time proceeds ($t \rightarrow +\infty$), a new stem structure S_1 forms and elongates, reconnecting these pairs of V-shaped solitons. This is the full process of the soliton reconnection induced by the 2-resonance.

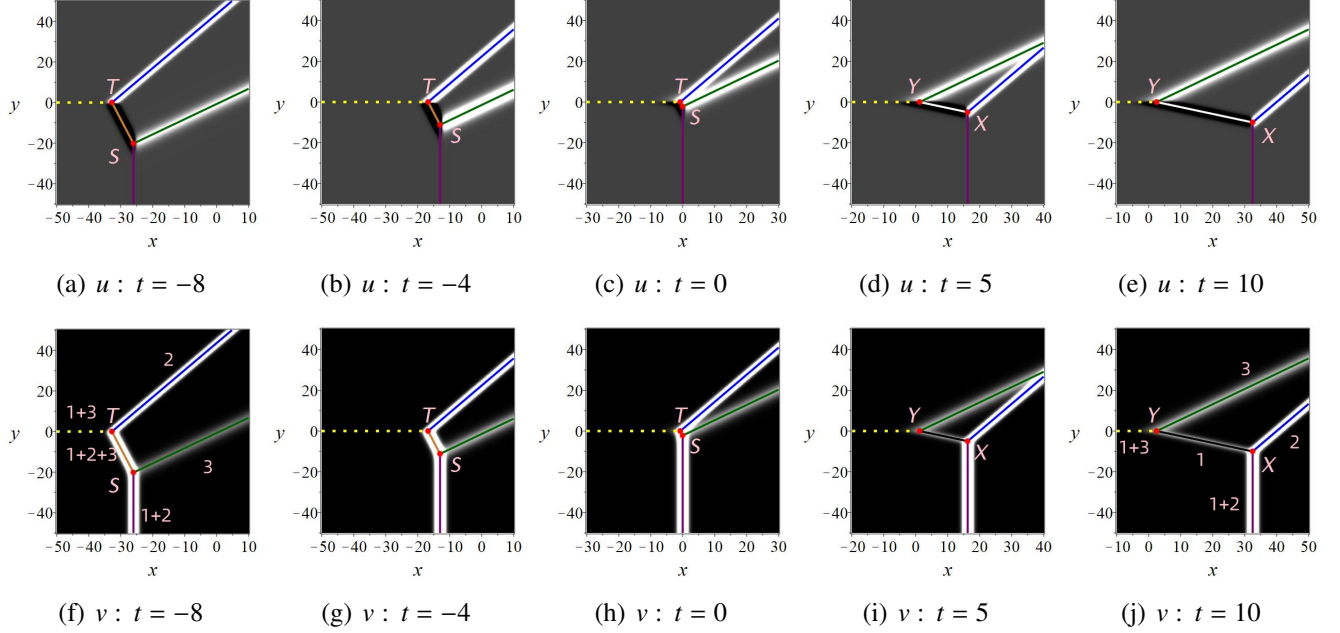


Figure 5: The density plots of the strong 2-resonant 3-soliton given by (2.1) and (4.1) with $k_1 = \frac{1}{2}$, $k_2 = 2$, $k_3 = -\frac{1}{2}$, $p_1 = \frac{3}{2}$, $p_2 = -\frac{3}{2}$, $p_3 = \frac{2}{3}$, $\xi_1^0 = 0$, $\xi_2^0 = 0$, $\xi_3^0 = 0$. The lines are the trajectories of the arms and stem structures, and the points are the endpoints of the variable length stem structures.

4.2. The stem structures with $0 < k_1 = -k_3 < k_2$, $p_1 = -p_2 > p_3 > 0$

The trajectory, amplitude, and velocity of the four arms and two stems are outlined in Tables 1 and 4, where the trajectories are given by (3.9) and below formulas,

$$l_{1+2}: \xi_1 + \xi_2 = 0, l_{1+3}: \xi_1 + \xi_3 = 0; \widehat{l_{1+2+3}}: \xi_1 + \xi_2 + \xi_3 + \ln a_{23} = 0. \quad (4.7)$$

It's easy to demonstrate that the trajectories of S_{1+2} , S_3 , and S_{1+2+3} intersect at a single point, and that the trajectories of S_2 , S_{1+3} , and S_{1+2+3} intersect at a single point as $t \rightarrow -\infty$. Similarly, the trajectories of S_1 , S_3 , and S_{1+3} intersect at a single point, and the trajectories of S_1 , S_2 , and S_{1+2} intersect at a single point as $t \rightarrow +\infty$. This further confirms the accuracy of the stem structure positions given in (4.6). It is noted that S_{1+3} has a vertical orientation, while S_{1+2} has a horizontal alignment. The trajectories of the arms and stem structures are illustrated in Fig. 5. By solving for the intersection points of these trajectories, the

endpoints of the variable-length stem structures can be determined as follows:

$$\begin{aligned} S & \left(\frac{(p_1 + p_2)(h_3 + \ln a_{23}) - p_3(h_1 + h_2)}{p_3(k_1 + k_2) - k_3(p_1 + p_2)}, \frac{-(k_1 + k_2)(h_3 + \ln a_{23}) + k_3(h_1 + h_2)}{p_3(k_1 + k_2) - k_3(p_1 + p_2)} \right), \\ T & \left(\frac{(p_1 + p_3)(h_2 + \ln a_{23}) - p_2(h_1 + h_3)}{p_2(k_1 + k_3) - k_2(p_1 + p_3)}, \frac{-(k_1 + k_3)(h_2 + \ln a_{23}) + k_2(h_1 + h_3)}{p_2(k_1 + k_3) - k_2(p_1 + p_3)} \right), \\ X & \left(\frac{p_1 h_2 - p_2 h_1}{p_2 k_1 - p_1 k_2}, \frac{-k_1 h_2 + k_2 h_1}{p_2 k_1 - p_1 k_2} \right), \quad Y \left(\frac{p_1 h_3 - p_3 h_1}{p_3 k_1 - p_1 k_3}, \frac{-k_1 h_3 + k_3 h_1}{p_3 k_1 - p_1 k_3} \right), \end{aligned} \quad (4.8)$$

where $h_1 = -k_1^3 t + \xi_1^0$, $h_2 = -k_2^3 t + \xi_2^0$, $h_3 = -k_3^3 t + \xi_3^0$. “S” and “T” respectively are the intersections of l_{1+2} , $\widehat{l_3}$ and $\widehat{l_2}$, $\widehat{l_{1+2+3}}$ at $t \ll 0$, while “X” and “Y” respectively are the intersections of l_{1+2} , l_2 and l_1 , l_3 at $t \gg 0$. Whereupon, the lengths of the variable length stem structures are obtained as following,

$$\begin{aligned} |ST| &= \left| \frac{(k_2 p_3 - k_3 p_2)(h_1 - \ln a_{23}) + (k_3 p_1 - k_1 p_3)(h_2 + \ln a_{23}) + (k_1 p_2 - k_2 p_1)(h_3 + \ln a_{23})}{(p_3(k_1 + k_2) - k_3(p_1 + p_2))(p_2(k_1 + k_3) - k_2(p_1 + p_3))} \right| \\ &\quad \cdot \sqrt{(k_1 + k_2 + k_3)^2 + (p_1 + p_2 + p_3)^2}, \\ |XY| &= \left| \frac{(k_2 p_3 - k_3 p_2)h_1 + (k_3 p_1 - k_1 p_3)h_2 + (k_1 p_2 - k_2 p_1)h_3}{(k_1 p_2 - k_2 p_1)(k_1 p_3 - k_3 p_1)} \right| \cdot \sqrt{k_1^2 + p_1^2}. \end{aligned} \quad (4.9)$$

Remark 4.2. Due to the intricate nature of the evolution around $t = 0$, the expressions (4.8) and (4.9) are applicable exclusively in the regimes where $t \ll 0$ and $t \gg 0$.

Then we consider how the amplitudes of the variable length stem structures change over time. As the correlation analysis approaches for u and v are largely the same, only the analysis of v is conducted herein. Subsequent sections present solely the formulas associated with v , while those pertaining to u are available in the appendix. For ease of calculation, we set $k_1 = \frac{1}{2}$, $k_2 = 2$, $k_3 = -\frac{1}{2}$, $p_1 = \frac{3}{2}$, $p_2 = -\frac{3}{2}$, $p_3 = \frac{2}{3}$, $\xi_1^0 = 0$, $\xi_2^0 = 0$, $\xi_3^0 = 0$. The cross-sectional curves of 3-soliton (2.1) with Eqs. (4.1) along $\widehat{l_{1+2+3}}$ shown in Fig. 6 (a) and (b) and l_1 are expressed as,

$$\begin{aligned} v|_{\widehat{l_{1+2+3}}}^{(1)} &= -\frac{169 \left(48 \sqrt{39} e^{\frac{15t}{4} + \frac{y}{2}} + 13\beta_1 e^{\frac{15t}{8} + \frac{7y}{2}} + 205\beta_1 e^{\frac{15t}{8} + \frac{4y}{3}} + 78\beta_1 e^{\frac{15t}{8} - \frac{5y}{6}} + 2704e^{\frac{13y}{6}} + 2704 \right)}{2 \left(13\beta_1 e^{\frac{15t}{8} + \frac{4y}{3}} + 3\beta_1 e^{\frac{15t}{8} - \frac{5y}{6}} + 169e^{\frac{13y}{6}} + 338 \right)^2}, \\ v|_{l_1}^{(1)} &= -\frac{1200e^{-\frac{143t}{18} + \frac{16x}{9}} + 39e^{-\frac{1157t}{72} + \frac{77x}{18}} + 624e^{-\frac{559t}{72} + \frac{19x}{18}} + 369e^{-\frac{65t}{8} + \frac{5x}{2}} + 9e^{\frac{13t}{72} - \frac{13x}{18}} + 9}{2 \left(3e^{-\frac{65t}{8} + \frac{5x}{2}} + 3e^{\frac{13t}{72} - \frac{13x}{18}} + 13e^{-\frac{143t}{18} + \frac{16x}{9}} + 6 \right)^2}, \end{aligned} \quad (4.10)$$

where, $\beta_1 = 13^{\frac{3}{4}} \cdot 3^{\frac{1}{4}}$.

The amplitudes of $u(R_5)$ and $u(R_6)$ are not given explicitly for the same reasons as the previous section. We just show the amplitudes of S_{1+2+3} and S_1 for u in Fig. 7 and mainly discuss v . The amplitudes of R_5 and R_6 for v are given as following,

$$\begin{aligned} S_{1+2+3} : v(R_5) &= -\frac{13 \left(9\beta_2 e^{\frac{93t}{16}} + 624\beta_2 e^{\frac{69t}{16}} + 615\beta_1 e^{\frac{27t}{8}} + 624\beta_3 e^{\frac{39t}{16}} + 4394\beta_3 e^{\frac{15t}{16}} + 35152 \right)}{2 \left(3\beta_1 e^{\frac{27t}{8}} + 3\beta_3 e^{\frac{39t}{16}} + 13\beta_3 e^{\frac{15t}{16}} + 338 \right)^2}, \\ S_1 : v(R_6) &= -\frac{3 \left(13e^{-\frac{103t}{12}} + 208e^{-\frac{71t}{12}} + 400e^{-\frac{29t}{6}} + 123e^{-\frac{15t}{4}} + 3e^{-\frac{13t}{12}} + 3 \right)}{2 \left(6 + 3e^{-\frac{15t}{4}} + 3e^{-\frac{13t}{12}} + 13e^{-\frac{29t}{6}} \right)^2}, \end{aligned} \quad (4.11)$$

where, $\beta_1 = 13^{\frac{3}{4}} \cdot 3^{\frac{1}{4}}$, $\beta_2 = 13^{\frac{1}{8}} \cdot 3^{\frac{7}{8}}$, $\beta_3 = 13^{\frac{3}{8}} \cdot 3^{\frac{5}{8}}$.

It is straight forward to determine the limits:

$$\lim_{t \rightarrow +\infty} v(R_5) = 0, \lim_{t \rightarrow -\infty} v(R_5) = -2, \lim_{t \rightarrow +\infty} v(R_6) = -\frac{1}{8}, \lim_{t \rightarrow -\infty} v(R_6) = 0.$$

These results are exhibited by Fig. 7. As can be seen from the figure that the evolution of arms around $t = 0$ is complicated. The figure also confirms that S_{1+2+3} disappears around $t = 0$ ($v(R_5) \approx 0$), and S_1 arises ($v(R_6) \approx 0$).

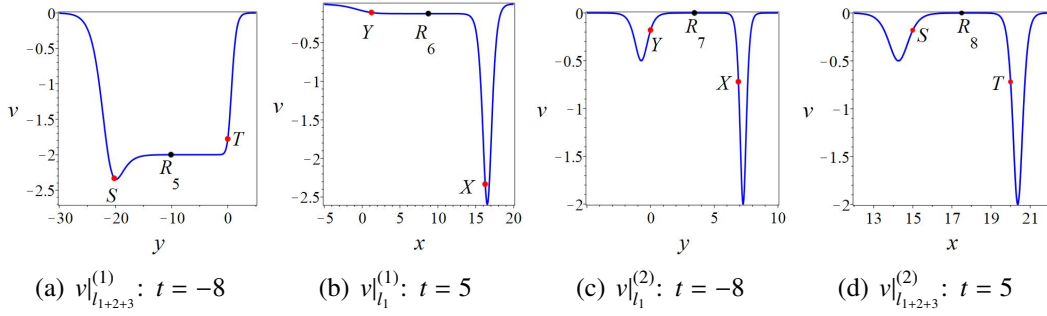


Figure 6: (a) (b) The cross-sectional curves (4.10); (c) (d) The cross-sectional curves (4.15). The red points are the endpoints of the variable length stem structures.

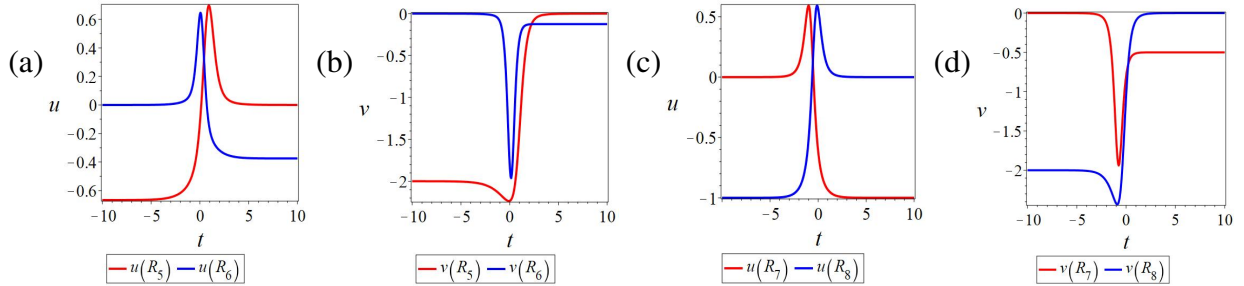


Figure 7: The evolutions of the amputation on the point R_j over time: (a)–(d) correspond to (5.6) (4.11) (5.8)(4.16), respectively.

Table 5: Physical quantities of the arms with $k_1 = -k_2 > k_3 > 0$, $0 < p_1 = -p_3 < p_2$

Soliton	Trajectory	Velocity	Amplitude	Components
S_{1+2}	l_{1+2}	$(0, 0)$	0	u_{1+2}
			0	v_{1+2}
S_{1+3}	l_{1+3}	$(k_1^2 - k_1 k_3 + k_3^2, 0)$	0	u_{1+3}
			$-\frac{(k_1+k_3)^2}{2}$	v_{1+3}
S_{1+2+3}	l_{1+2+3}	$(k_3^2, -\frac{k_3^3}{p_2})$	$\frac{k_3 p_2}{2}$	$\widehat{u_{1+2+3}}$
			$-\frac{k_3^2}{2}$	$\widehat{v_{1+2+3}}$

The solitons S_j ($j = 1 + 2, 1 + 3, 1 + 2 + 3$) are composed by two components u_j and v_j , and their trajectories are listed by (4.7).

4.3. *The asymptotic analysis and stem structures with $k_1 = -k_2 > k_3 > 0$, $0 < p_1 = -p_3 < p_2$*

Using the same approach as outlined in the previous section, we arrive at the following proposition.

Proposition 4.3. *The asymptotic forms of the strong 2-resonant 3-soliton with $k_1 = -k_2 > k_3 > 0$, $0 < p_1 = -p_3 < p_2$ are as following:*

Before collision ($t \rightarrow -\infty$):

$$\begin{aligned}
 y \rightarrow +\infty, S_2 : \quad u_2 &\approx -\frac{k_2 p_2}{2} \operatorname{sech}^2\left(\frac{\xi_2}{2}\right), \quad v_2 \approx -\frac{k_2^2}{2} \operatorname{sech}^2\left(\frac{\xi_2}{2}\right), \\
 S_3 : \quad u_3 &\approx -\frac{k_3 p_3}{2} \operatorname{sech}^2\left(\frac{\xi_3}{2}\right), \quad v_3 \approx -\frac{k_3^2}{2} \operatorname{sech}^2\left(\frac{\xi_3}{2}\right), \\
 y \rightarrow -\infty, S_{1+2} : \quad u_{1+2} &\approx -\frac{(k_1 + k_2)(p_1 + p_2)}{2} \operatorname{sech}^2\left(\frac{\xi_1 + \xi_2}{2}\right), \quad v_{1+2} \approx -\frac{(k_1 + k_2)^2}{2} \operatorname{sech}^2\left(\frac{\xi_1 + \xi_2}{2}\right), \\
 x \rightarrow -\infty, S_{1+3} : \quad u_{1+3} &\approx -\frac{(k_1 + k_3)(p_1 + p_3)}{2} \operatorname{sech}^2\left(\frac{\xi_1 + \xi_3}{2}\right), \quad v_{1+3} \approx -\frac{(k_1 + k_3)^2}{2} \operatorname{sech}^2\left(\frac{\xi_1 + \xi_3}{2}\right).
 \end{aligned} \tag{4.12}$$

After collision ($t \rightarrow +\infty$):

$$\begin{aligned}
 y \rightarrow +\infty, S_2 : \quad \widehat{u}_2 &\approx -\frac{k_2 p_2}{2} \operatorname{sech}^2\left(\frac{\xi_2 + \ln a_{23}}{2}\right), \quad \widehat{v}_2 \approx -\frac{k_2^2}{2} \operatorname{sech}^2\left(\frac{\xi_2}{2}\right), \\
 S_3 : \quad \widehat{u}_3 &\approx -\frac{k_3 p_3}{2} \operatorname{sech}^2\left(\frac{\xi_3 + \ln a_{23}}{2}\right), \quad \widehat{v}_3 \approx -\frac{k_3^2}{2} \operatorname{sech}^2\left(\frac{\xi_3 + \ln a_{23}}{2}\right), \\
 y \rightarrow -\infty, S_{1+2} : \quad u_{1+2} &\approx -\frac{(k_1 + k_2)(p_1 + p_2)}{2} \operatorname{sech}^2\left(\frac{\xi_1 + \xi_2}{2}\right), \quad v_{1+2} \approx -\frac{(k_1 + k_2)^2}{2} \operatorname{sech}^2\left(\frac{\xi_1 + \xi_2}{2}\right), \\
 x \rightarrow -\infty, S_{1+3} : \quad u_{1+3} &\approx -\frac{(k_1 + k_3)(p_1 + p_3)}{2} \operatorname{sech}^2\left(\frac{\xi_1 + \xi_3}{2}\right), \quad v_{1+3} \approx -\frac{(k_1 + k_3)^2}{2} \operatorname{sech}^2\left(\frac{\xi_1 + \xi_3}{2}\right).
 \end{aligned} \tag{4.13}$$

Proposition 4.4. *The stem structures corresponding to asymptotic forms (4.12) and (4.13) are as following:*

$$\begin{aligned}
 t \rightarrow -\infty, S_1 : \quad u_1 &\approx -\frac{k_1 p_1}{2} \operatorname{sech}^2\left(\frac{\xi_1}{2}\right), \quad v_1 \approx -\frac{k_1^2}{2} \operatorname{sech}^2\left(\frac{\xi_1}{2}\right), \\
 t \rightarrow +\infty, S_{1+2+3} : \quad \widehat{u_{1+2+3}} &\approx -\frac{(k_1 + k_2 + k_3)(p_1 + p_2 + p_3)}{2} \operatorname{sech}^2\left(\frac{\xi_1 + \xi_2 + \xi_3 + \ln a_{23}}{2}\right), \\
 \widehat{v_{1+2+3}} &\approx -\frac{(k_1 + k_2 + k_3)^2}{2} \operatorname{sech}^2\left(\frac{\xi_1 + \xi_2 + \xi_3}{2}\right).
 \end{aligned} \tag{4.14}$$

The trajectory, amplitude, and velocity of the arms are presented in detail in Tables 1 and 5. It is evident from the data that the amplitudes of v_{1+2} , u_{1+2} , and u_{1+3} are all zero, signifying that u displays three arms while v shows four arms. The background plane is represented by density plots, providing a visual context, with the trajectories of the arms indicated by lines. Initially, as $t \rightarrow -\infty$, S_1 appears as a stem structure of variable length. As time progresses, the length of S_1 decreases, and the distances between S_2 , S_3 , and S_{1+3} reduce. Near $t = 0$, S_1 disappears, giving rise to a new stem structure S_{1+2+3} , while S_2 and S_3 continue their movement. During this transformation, the arms of v undergo exchanges and reconnections. Early on, as $t \rightarrow +\infty$, one end of the variable length stem structure S_1 connects with S_{1+2} , while the other end links with S_3 and S_{1+3} . As time advances toward $t \gg 0$, the stem structure S_{1+2+3} connects with S_3 at one end, and with S_2 and S_{1+3} at the other. The endpoints of these variable length stem structures can be determined using the same method as previously described, resulting in expressions

identical to (4.8), illustrated as red points in Fig. 8. Consequently, the lengths of the trajectories of these stem structures remain consistent with Eq. (4.9).

Next, we explore the temporal evolution of the amplitudes of the variable length stem structures. Similarly to the preceding section, next we will focus on discussing v for simplicity and the formula corresponding to u are provided in the appendix. To facilitate computation, we set $k_1 = 2$, $k_2 = -2$, $k_3 = 1$, $p_1 = 1$, $p_2 = 2$, $p_3 = -1$, $\xi_1^0 = 0$, $\xi_2^0 = 0$, and $\xi_3^0 = 0$. The cross-sectional curves of 3-soliton (2.1) with Eqs. (4.1) along l_1 and $\widehat{l_{1+2+3}}$ shown in Fig. 6 (c) and (d) are expressed as,

$$\begin{aligned} v|_{l_1}^{(2)} &= -18 \frac{59049 e^{12t+6y} + 59049 e^{12t+9y} + 1053 e^{6t} + 4374 e^{6t+3y} + 2916 e^{6t+6y} + e^{-3y}}{(9 + 1458 e^{6t+3y} + 729 e^{6t+6y} + e^{-3y})^2}, \\ v|_{\widehat{l_{1+2+3}}}^{(2)} &= -\frac{54 e^{15t-3x} + 18 e^{39t-9x} + 72 e^{6t} + 8 e^{24t-6x} + 20 e^{-9t+3x} + 8}{(2 + e^{24t-6x} + e^{-9t+3x} + 9 e^{15t-3x})^2}. \end{aligned} \quad (4.15)$$

It is worth noting that the amplitudes under investigation in this context are the function values at points R_5 and R_6 . However, to avoid confusion with the previous discussion, we opt to re-designate these two points as R_7 and R_8 . Consequently, the amplitudes of R_7 and R_8 are given by:

$$\begin{aligned} S_{1+2+3} : \quad v(R_7) &= -\frac{6e^{\frac{3t}{2}} (81 \sqrt{3} e^{6t} + 729 e^{\frac{15t}{2}} + 162 \sqrt{3} e^{3t} + 351 e^{\frac{9t}{2}} + \sqrt{3} + 36e^{\frac{3t}{2}})}{(54 \sqrt{3} e^{\frac{9t}{2}} + \sqrt{3} e^{\frac{3t}{2}} + 9 e^{3t} + 3)^2}, \\ S_1 : \quad v(R_8) &= -\frac{18e^{\frac{15t}{2}} + 72 e^{6t} + 54 e^{\frac{9t}{2}} + 8 e^{3t} + 20 e^{\frac{3t}{2}} + 8}{(2 + e^{3t} + e^{\frac{3t}{2}} + 9 e^{\frac{9t}{2}})^2}. \end{aligned} \quad (4.16)$$

Easily obtain the limits as

$$\lim_{t \rightarrow +\infty} v(R_7) = -\frac{1}{2}, \quad \lim_{t \rightarrow -\infty} v(R_7) = 0, \quad \lim_{t \rightarrow +\infty} v(R_8) = 0, \quad \lim_{t \rightarrow -\infty} v(R_8) = -2.$$

This can also be confirmed in Fig. 7. The plots of $v(R_7)$ and $v(R_8)$ are depicted in Fig. 7 (d). It is evident that the evolution of variable length stem structures around $t = 0$ is intricate. The figure also corroborates the disappearance of S_1 around $t = 0$ (indicated by $v(R_8) \approx 0$), coinciding with the emergence of S_{1+2+3} ($v(R_7) \approx 0$).

5. Conclusions and discussions

This paper systematically studies the asymptotic forms and variable-length stem structures during soliton reconnection, specifically occurring in 2-resonance 3-solitons of the ANNV system (1.1). The construction method of the 2-resonant 3-soliton solution in this paper is different from that in Ref. [24], but similar to the solution in Ref. [24] (see its section 7.2: partial resonance solution). During soliton reconnection, two pairs of V-shaped solitons gradually approach, bounce off in another direction, and exhibit the gradual disappearance of one variable-length stem structure alongside the emergence of another (see Figs. 1, 4, 5, 8). We address two distinct cases of 2-resonances: $a_{12} = a_{13} = 0$, $0 < a_{23} < +\infty$ (weak 2-resonance) and $a_{12} = a_{13} = +\infty$, $0 < a_{23} < +\infty$ (strong 2-resonance).

Using two-variable asymptotic analysis method (see paragraph 3, section 3.1), we analytically derive the asymptotic forms of the four arms and stem structures of the 2-resonant 3-solitons as $t \rightarrow \pm\infty$. The weak 2-resonance case is presented in Propositions 3.1–3.4, while the strong 2-resonance case is introduced in Propositions 4.1–4.4. This analysis also provides a systematic mathematical theory of soliton reconnection. These analytical forms include formulas of the trajectories, amplitudes, and velocities of

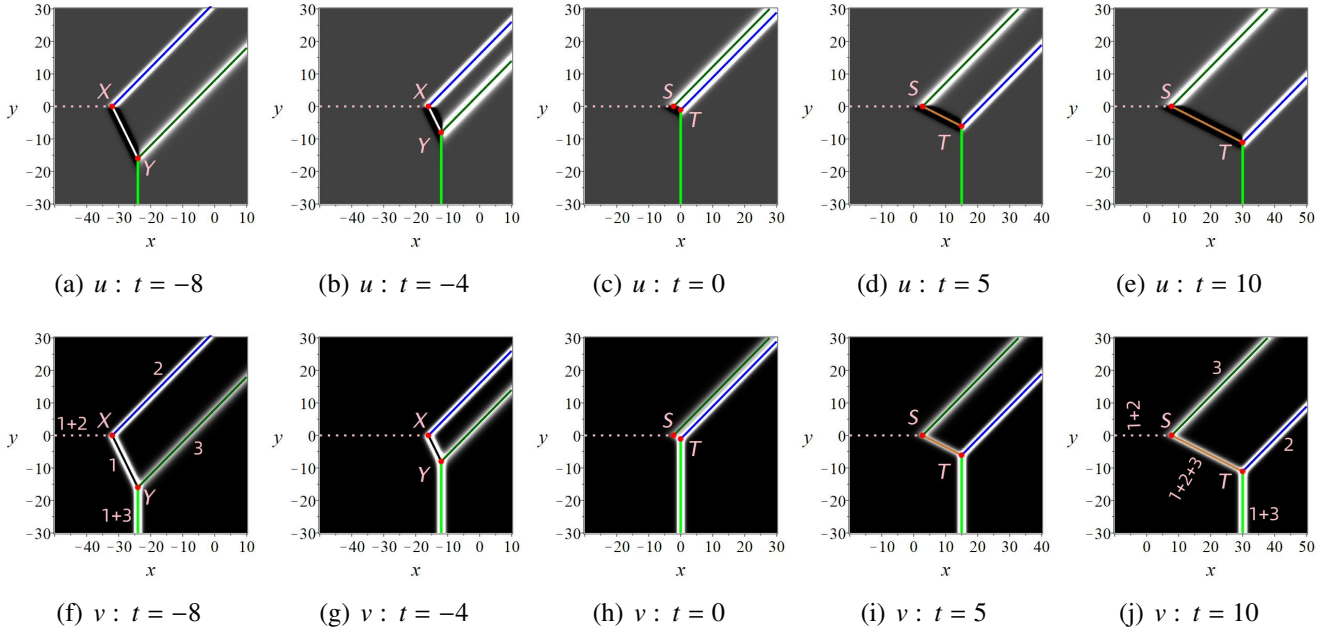


Figure 8: The density plots of the strong 2-resonant 3-soliton given by (2.1) and (4.1) with $k_1 = 2, k_2 = -2, k_3 = 1, p_1 = 1, p_2 = 2, p_3 = -1, \xi_1^0 = 0, \xi_2^0 = 0, \xi_3^0 = 0$. The lines are the trajectories of the arms and stem structures, and the points are the endpoints of the variable length stem structures.

the arms and stem structures. By combining the corresponding trajectories, we determine the vertices of the V-shaped solitons and define them as the endpoints of the stem structures, as shown in Eqs. (3.10), (3.17), and (4.8). We then provide formulas for the length of the stem structures in Eqs. (3.11), (3.18), and (4.9), reflecting the linear evolution of the stem lengths over time for $t \gg 0$ and $t \ll 0$.

Based on the asymptotic forms and stem structures studied in this paper, we observe the following facts:

- The 2-resonant 3-solitons of Eq. (1.1) possess four infinitely extending arms. Especially, owing to the constraint $0 < a_{23} < +\infty$, the arms S_2 and S_3 manifest a finite phase shift as $t \rightarrow \pm\infty$. Conversely, the remaining two arms remain unchanged throughout the collision ($t \rightarrow \pm\infty$). This represents a significant improvement over previous studies that only considered spatial progressive behavior.
- The 2-resonant 3-solitons of Eq. (1.1) exhibit distinct stem structures as $t \rightarrow -\infty$ and $+\infty$ respectively. Unlike the characteristics observed in the stem structures of quasi-resonant 2-solitons examined in Ref. [45], the local properties of the stem structure in soliton reconnections undergo temporal variations.
- The profile curve where the trajectory of the conventional stem structure (with non-zero amplitude) is located contains only extreme points, unlike the extreme lines found in line solitons. The location of these extreme points changes over time.

A natural extension of the present work would be to investigate partial and complete resonances of higher-order solitons. Increasing the number of a_{ij} parameters would give rise to a richer array of partial resonance cases, promising the emergence of more intriguing phenomena. We intend to explore this extension in future studies to provide a more in-depth understanding of the complexities inherent in the ANNV system and to extend our findings to other soliton equations.

Conflict statement The authors declare that they have no conflict of interests.

Data availability The data that support the findings of this study are available within the article.

Acknowledgments This work is supported by the National Natural Science Foundation of China (Grants 12071304, 12471239), NUPTSF (Grant NY222169), Shenzhen Natural Science Fund (the Stable Support Plan Program) (Grant 20220809163103001), and Guangdong Basic and Applied Basic Research Foundation (Grant 2024A1515013106)

Appendix

The cross-sectional curves of 3-soliton (2.1) with Eqs. (3.1) along l_{1-2} and l_{1-3} shown in Fig. 3 (a) and (b) are expressed as,

$$\begin{aligned} u|_{l_{1-2}}^{(1)} &= -\frac{13}{6} \cdot \frac{60e^{\frac{15t}{2} + \frac{11y}{3}} + 108e^{\frac{15t}{2} + \frac{17y}{6}} + 390e^{5t + \frac{13y}{6}} + 585e^{\frac{5t}{2} + \frac{3y}{2}} + 52e^{\frac{5t}{2} + \frac{2y}{3}}}{(3e^{5t + \frac{13y}{6}} + 26e^{\frac{5t}{2} + \frac{3y}{2}} + 13e^{\frac{5t}{2} + \frac{2y}{3}} + 13)^2}, \\ u|_{l_{1-3}}^{(1)} &= -\frac{13}{6} \cdot \frac{156e^{3x - \frac{33t}{4}} + 12e^{\frac{9x}{2} - \frac{129t}{8}} + 390e^{\frac{5x}{2} - \frac{65t}{8}} + 169e^{\frac{x}{2} - \frac{t}{8}} + 468e^{2x - 8t}}{(3e^{\frac{5x}{2} - \frac{65t}{8}} + 26e^{\frac{x}{2} - \frac{t}{8}} + 13e^{2x - 8t} + 13)^2}. \end{aligned} \quad (5.1)$$

The amplitudes of S_{1-2} and S_{1-3} are expressed as:

$$\begin{aligned} S_{1-2} : u(R_1) &= -\frac{3}{2} \cdot \frac{468\gamma_2 e^{\frac{325t}{144}} + 585\gamma_2 e^{\frac{125t}{144}} + 12\gamma_4 e^{\frac{25t}{8}} + 390\gamma_1 e^{\frac{25t}{16}} + 260\gamma_3}{(3\gamma_4 e^{\frac{325t}{144}} + 3\gamma_1 e^{\frac{25t}{36}} + 9e^{\frac{25t}{16}} + 26\gamma_2)^2}, \\ S_{1-3} : u(R_2) &= -\frac{2197\gamma_4 e^{\frac{75t}{16}} + 2028\gamma_3 e^{\frac{45t}{8}} + 5070\gamma_1 e^{\frac{75t}{16}} + 6084\gamma_4 e^{\frac{60t}{16}} + 676\gamma_2 e^{\frac{15t}{16}}}{2(26\gamma_2 e^{\frac{75t}{16}} + 39e^{\frac{15t}{4}} + 3\gamma_1 e^{\frac{15t}{16}} + 13\gamma_4)^2}, \end{aligned} \quad (5.2)$$

where $\gamma_1 = 3^{\frac{3}{8}} \cdot 13^{\frac{5}{8}}$, $\gamma_2 = 3^{\frac{7}{8}} \cdot 13^{\frac{1}{8}}$, $\gamma_3 = 3^{\frac{1}{4}} \cdot 13^{\frac{3}{4}}$, $\gamma_4 = \sqrt{39}$.

The cross-sectional curves of 3-soliton (2.1) with Eqs. (3.1) along l_{1-2} and l_{1-3} are expressed as,

$$\begin{aligned} u|_{l_{1-2}}^{(2)} &= -\frac{75e^{5x-17t} + 90e^{4x-10t} + 450e^{3x-9t} + 2250e^{2x-8t} + 450e^{x-t}}{(e^{3x-9t} + 30e^{2x-8t} + 15e^{x-t} + 15)^2}, \\ u|_{l_{1-3}}^{(2)} &= -\frac{75e^{5x-17t} + 90e^{4x-10t} + 450e^{3x-9t} + 2250e^{2x-8t} + 450e^{x-t}}{(e^{3x-9t} + 30e^{2x-8t} + 15e^{x-t} + 15)^2}. \end{aligned} \quad (5.3)$$

The amplitudes of the variable length stem structures, respectively, are

$$\begin{aligned} S_{1-2} : u(R_3) &= -\frac{90e^{6t} + 2\alpha_6 e^{\frac{15t}{2}} + 30\alpha_6 e^{\frac{9t}{2}} + 150e^{3t} + 75\alpha_6 e^{\frac{3t}{2}}}{(\alpha_6 e^{\frac{9t}{2}} + \alpha_6 e^{\frac{3t}{2}} + e^{3t} + 30)^2}, \\ S_{1-3} : u(R_4) &= -\frac{225(9\alpha_8 e^{\frac{7t}{2}} + 6\alpha_7 e^{4t} + 2\alpha_6 \alpha_7 e^{\frac{5t}{2}} + 6\alpha_6 e^{\frac{3t}{2}} + 2\alpha_7 e^t)}{(30\alpha_7 e^{\frac{5t}{2}} + \alpha_6 \alpha_7 e^t + 15e^{\frac{3t}{2}} + 15\alpha_6)^2}, \end{aligned} \quad (5.4)$$

where $\alpha_6 = \sqrt{15}$, $\alpha_7 = \sqrt[3]{15}$, $\alpha_8 = \sqrt[6]{15}$.

The cross-sectional curves of 3-soliton (2.1) with Eqs. (4.1) along $\widehat{l_{1+2+3}}$ and l_1 are expressed as,

$$u|_{\widehat{l_{1+2+3}}}^{(1)} = \frac{169 \left(108 \sqrt{39} e^{\frac{15t}{4} + \frac{y}{2}} + 52\beta_1 e^{\frac{15t}{8} + \frac{7y}{2}} + 273\beta_1 e^{\frac{15t}{8} + \frac{4y}{3}} + 12\beta_1 e^{\frac{15t}{8} - \frac{5y}{6}} + 6084e^{\frac{13y}{6}} - 2704 \right)}{6 \left(13\beta_1 e^{\frac{15t}{8} + \frac{4y}{3}} + 3\beta_1 e^{\frac{15t}{8} - \frac{5y}{6}} + 169e^{\frac{13y}{6}} + 338 \right)^2},$$

$$u|_{l_1}^{(1)} = \frac{108e^{-\frac{65t}{8} + \frac{5x}{2}} + 468e^{-\frac{559t}{72} + \frac{19x}{18}} + 182e^{-\frac{143t}{18} + \frac{16x}{9}} + 52e^{-\frac{1157t}{72} + \frac{77x}{18}} + 12e^{\frac{13t}{72} - \frac{13x}{18}} - 27}{2 \left(3e^{-\frac{65t}{8} + \frac{5x}{2}} + 13e^{-\frac{143t}{18} + \frac{16x}{9}} + 3e^{\frac{13t}{72} - \frac{13x}{18}} + 6 \right)^2},$$
(5.5)

where, $\beta_1 = 13^{\frac{3}{4}} \cdot 3^{\frac{1}{4}}$.

The amplitudes of R_5 and R_6 for u are given as following,

$$S_{1+2+3} : u(R_5) = \frac{13 \left(36\beta_2 e^{\frac{93t}{16}} + 1404\beta_2 e^{\frac{69t}{16}} + 819\beta_1 e^{\frac{27t}{8}} + 1404\beta_3 e^{\frac{39t}{16}} + 676\beta_3 e^{\frac{15t}{16}} - 35152 \right)}{6 \left(3\beta_1 e^{\frac{27t}{8}} + 3\beta_3 e^{\frac{39t}{16}} + 13\beta_3 e^{\frac{15t}{16}} + 338 \right)^2},$$

$$S_1 : u(R_6) = \frac{108e^{-\frac{15t}{4}} + 468e^{-\frac{71t}{12}} + 182e^{-\frac{29t}{6}} + 52e^{-\frac{103t}{12}} + 12e^{-\frac{13t}{12}} - 27}{2 \left(3e^{-\frac{15t}{4}} + 13e^{-\frac{29t}{6}} + 3e^{-\frac{13t}{12}} + 6 \right)^2},$$
(5.6)

where, $\beta_1 = 13^{\frac{3}{4}} \cdot 3^{\frac{1}{4}}$, $\beta_2 = 13^{\frac{1}{8}} \cdot 3^{\frac{7}{8}}$, $\beta_3 = 13^{\frac{3}{8}} \cdot 3^{\frac{5}{8}}$.

The cross-sectional curves of 3-soliton (2.1) with Eqs. (4.1) along l_1 and $\widehat{l_{1+2+3}}$ for u are expressed as,

$$u|_{l_1}^{(2)} = \frac{59049e^{3y} + e^{-12t-9y} + 324e^{-6t-6y} + 2916e^{-6t} - 118098}{(e^{-6t-6y} + 9e^{-6t-3y} + 729e^{3y} + 1458)^2},$$

$$u|_{\widehat{l_{1+2+3}}}^{(2)} = \frac{59049e^{3y} + e^{-12t-9y} + 324e^{-6t-6y} + 2916e^{-6t} - 118098}{(e^{-6t-6y} + 9e^{-6t-3y} + 729e^{3y} + 1458)^2}.$$
(5.7)

The amplitudes of R_7 and R_8 are given by:

$$S_{1+2+3} : u(R_7) = \frac{2 \sqrt{3} e^{-\frac{15t}{2}} + 72e^{-6t} + 216e^{-3t} + 162 \sqrt{3} e^{-\frac{3t}{2}} - 2916}{\left(\sqrt{3} e^{-\frac{9t}{2}} + 3 \sqrt{3} e^{-\frac{3t}{2}} + e^{-3t} + 54 \right)^2},$$

$$S_1 : u(R_8) = \frac{72e^{6t} + 18e^{\frac{15t}{2}} + 9e^{\frac{9t}{2}} + 8e^{3t} + 2e^{\frac{3t}{2}} - 4}{\left(9e^{\frac{9t}{2}} + e^{3t} + e^{\frac{3t}{2}} + 2 \right)^2}.$$
(5.8)

References

- [1] J. S. Russell, Report on waves, Report of fourteenth meeting of British Association for the Advancement of Science, York, 1844, London: John Murray, 311–390
- [2] D. J. Korteweg, G. de Vries, XLI. On the change of form of long waves advancing in a rectangular canal, and on a new type of long stationary waves, Philos. Mag. 39 (1895), 422–443
- [3] M. J. Ablowitz, P. A. Clarkson, Solitons: nonlinear evolution equations and inverse scattering. (Cambridge University Press, Cambridge, 1991)
- [4] C. S. Gardner, J. M. Greene, M. D. Kruskal, R. M. Miura, Korteweg-deVries equation and generalizations VI: methods for exact solution. Comm. Pure Appl. Math. 27, 97–133 (1974)
- [5] M. J. Ablowitz and H. Segur, Solitons and the Inverse Scattering Transform (SIAM, Philadelphia, 1981)

- [6] A. C. Newell, Solitons in Mathematics and Physics (Society for Industrial and Applied Mathematics, Philadelphia, 1985)
- [7] N. Zabusky and M. Kruskal, Interaction of solitons in a collisionless plasma and the recurrence of initial states, *Phys. Rev. Lett.* 15, 240 (1965)
- [8] C. S. Gardner, J. M. Greene, M. D. Kruskal, R. M. Miura, Method for solving the Korteweg-de Vries equation, *Phys. Rev. Lett.* 19, 1095–1097 (1967)
- [9] V. B. Matveev and M. A. Salle, Darboux Transformations and Solitons (Springer-Verlag, Berlin, 1991)
- [10] C. H. Gu, H. S. Hu, Z. X. Zhou, Darboux Transformations in Integrable Systems, (Springer, Dordrecht, 2006)
- [11] J. S. He, L. Zhang, Y. Cheng, Y. S. Li, Determinant representation of Darboux transformation for the AKNS system, *Science in China Series A-Mathematics*, 49, 1867–1878 (2006)
- [12] R. Hirota, Exact solution of the Korteweg-de Vries equation for multiple collisions of solitons, *Phys. Rev. Lett.* 27, 1192–1194 (1971)
- [13] R. Hirota, The direct method in soliton theory (Cambridge: Cambridge University Press, 2004)
- [14] Y. Jiang, B. Tian, W. J. Liu, et al. Soliton interactions and complexes for coupled nonlinear Schrödinger equations, *Phys. Rev. E* 85, 036605 (2012)
- [15] N. Akhmediev and A. Ankiewicz, Dissipative solitons, (Springer, Berlin, 2005)
- [16] G. I. Stegeman and M. Segev, Optical spatial solitons and their interactions: Universality and diversity, *Science* 286, 1518 (1999)
- [17] J. Miles, Resonantly interacting solitary waves, *J. Fluid Mech.* 79, 171–179 (1977)
- [18] A. C. Newell and L. G. Redekopp, Breakdown of Zakharov-Shabat theory and soliton creation, *Phys. Rev. Lett.* 38, 377–380 (1977)
- [19] K. Ohkuma and M. Wadati, The Kadomtsev-Petviashvili equation: the trace method and the soliton resonances, *J. Phys. Soc. Japan*, 52, 749–760 (1983)
- [20] O. K. Pashaev and M. L. Y. Francisco, Degenerate four-virtual-soliton resonance for the KP-II, *Theor. Math. Phys.* 144, 1022–1029 (2005)
- [21] G. Biondini, K. I. Maruno, M. Oikawa, and H. Tsuji, Soliton Interactions of the Kadomtsev-Petviashvili Equation and Generation of Large-Amplitude Water Waves, *Stud. Appl. Math.* 122, 377–394 (2009)
- [22] F. Kako, N. Yajima, Interaction of Ion-Acoustic solitons in two-dimensional Space, *J. Phys. Soc. Japan* 49, 2063–2071 (1980)
- [23] M. J. Ablowitz and D. E. Baldwin, Nonlinear shallow ocean-wave soliton interactions on flat beaches, *Phys. Rev. E* 86, 036305 (2012)
- [24] G. Biondini, D. Kireyev and K. Maruno, Soliton resonance and web structure in the Davey-Stewartson system, *J. Phys. A: Math. Theor.* 55, 305701 (2022)
- [25] J. G. Rao, T. Kanna, J. S. He, A study on resonant collision in the two-dimensional multi-component long-wave-short-wave resonance system, *Proc. R. Soc. A* 478, 20210777 (2022)
- [26] H. Yeh, W. Li, and Y. Kodama, Mach reflection and KP solitons in shallow water, *Eur. Phys. J. Special Edition* 185, 97 (2010).
- [27] T. Maxworthy, On the formation of nonlinear internal waves from the gravitational collapse of mixed regions in two and three dimensions, *J. Fluid Mech.* 96, 47–64 (1980)
- [28] K. Nishinari, K. Abe and J. Satsuma, A new-type of soliton behavior in a two dimensional plasma system, *J. Phys. Soc. Japan* 62, 2021–2029 (1993)

- [29] E. Medina, An n soliton resonance solution for the KP equation: Interaction with change of form and velocity, *Lett. Math. Phys.* 62, 91–99 (2002)
- [30] W. S. Duan, Y. R. Shi, X. R. Hong, Theoretical study of resonance of the Kadomtsev-Petviashvili equation, *Phys. Lett. A* 323, 89–94 (2004)
- [31] Y. Shen, B. Tian, T. Y. Zhou, X. T. Gao, Shallow-water-wave studies on a (2+1)-dimensional Hirota-Satsuma-Ito system: X-type soliton, resonant Y-type soliton and hybrid solutions, *Chaos Solitons Fractals* 157, 111861 (2022)
- [32] S. J. Ryskamp, M. A. Hoefer and G. Biondini, Modulation theory for soliton resonance and Mach reflection, *Proc. R. Soc. A* 478, 20210823 (2022)
- [33] M. L. Y. Francisco, J. H. Lee, O. K. Pashaev, Dissipative hierarchies and resonance solitons for KP-II and MKP-II, *Math. Comput. Simul.* 74, 323–332 (2007)
- [34] Y. Kodama, KP solitons in shallow water, *J. Phys. A: Math. Theor.* 43, 434004 (2010)
- [35] S. Y. Lou and X. B. Hu, Infinitely many Lax pairs and symmetry constraints of the KP equation, *J. Math. Phys.* 38, 6401 (1997)
- [36] P. G. Estévez and S. Leble, A wave equation in 2+1: painleve analysis and solutions, *Inverse Problems* 11, 925 (1995)
- [37] M. Boiti, J. J. P. Leon, M. Manna and F. Pempinelli, On the spectral transform of a Korteweg-de Vries equation in two spatial dimensions, *Inverse Problems* 2, 271 (1986)
- [38] P. A. Clarkson and E. L. Mansfield, On a shallow wave equation, *Nonlinearity* 7, 795 (1994)
- [39] H. Y. Ruan and Y. X. Chen, Restudy of the structures and interactions of the soliton in the asymmetric Nizhnik-Novikov-Veselov equation, *J. Phys. A: Math. Gen.* 37, 2709 (2004)
- [40] E. Fan, Quasi-periodic waves and an asymptotic property for the asymmetrical Nizhnik-Novikov-Veselov equation, *J. Phys. A: Math. Theor.* 42, 095206 (2009)
- [41] A. M. Wazwaz, Structures of multiple soliton solutions of the generalized, asymmetric and modified Nizhnik-Novikov-Veselov equations, *Appl. Math. Comput.* 218, 11344–11349 (2012)
- [42] J. Manafian, O. A. Ilhan, L. Avazpour, A. Alizadeh, N-lump and interaction solutions of localized waves to the (2+1)-dimensional asymmetrical Nizhnik-Novikov-Veselov equation arise from a model for an incompressible fluid, *Math. Meth. Appl. Sci.* 43, 9904–9927 (2020)
- [43] L. J. Guo, J. S. He, and D. Mihalache, Rational and semi-rational solutions to the asymmetric Nizhnik-Novikov-Veselov system, *J. Phys. A: Math. Theor.* 54, 095703 (2021)
- [44] L. J. Guo, L. H. Wang, L. Chen, J. S. He, Dynamics of the rogue lump in the asymmetric Nizhnik-Novikov-Veselov system, *Stud. Appl. Math.* 151, 35–59 (2023)
- [45] F. Yuan, J. G. Rao, J. S. He, Y. Cheng, Localized stem structures in quasi-resonant two-soliton solutions for the asymmetric Nizhnik-Novikov-Veselov system, *J. Math. Phys.* 65, 083508 (2024)
- [46] Y. Q. Yuan, X. H. Zhao, Resonant solitons of the B-type Kadomtsev-Petviashvili equation, *Phys. Lett. A* 458, 128592 (2023)
- [47] J. G. Rao, J. S. He, B. A. Malomed, Resonant collisions between lumps and periodic solitons in the Kadomtsev-Petviashvili I equation, *J. Math. Phys.* 63, 013510 (2022)
- [48] T. Xu, L. L. Li, M. Li, C. X. Li and X. F. Zhang, Rational solutions of the defocusing non-local nonlinear Schrödinger equation: asymptotic analysis and soliton interactions, *Proc. R. Soc. A* 477, 20210512 (2021)
- [49] R. Radha, M. Lakshmanan, Singularity analysis and localized coherent structures in (2+1)-dimensional generalized Korteweg-de Vries equations, *J. Math. Phys.* 35, 4746–4756 (1994)